Silver ion deposition on gold and silver disc electrodes from aqueous solutions and from dry or wet [EMIM][NTf2] room-temperature ionic liquid

Dongya Liu, Denise Krulic, Henri Groult, Nicolas Fatouros

Silver ion deposition on gold and silver disc electrodes from aqueous solutions and from dry or wet [EMIM][NTf$_2$] room-temperature ionic liquid

Dongya Liu, Denise Krulic[*], Henri Groult, Nicolas Fatouros

Sorbonne Universités, UPMC Univ Paris 06, CNRS, Laboratoire PHENIX, Electrochimie et Liquides Ioniques, Case 51, 4 place Jussieu, 75005 Paris, France

[*]Corresponding author. Tel.: +33 1 44 27 25 90
E-mail address: denise.krulic@upmc.fr

Abstract

Silver ion deposition on gold and silver disc electrodes in nitrate aqueous solutions and in [EMIM][NTf$_2$] room-temperature ionic liquid were investigated by staircase voltammetry (SV) and square wave voltammetry (SWV). The kinetics of the Ag(I)/Ag couple in [EMIM][NTf$_2$] solutions prepared with AgNTf$_2$ depends both on their water content and the AgNTf$_2$ concentration. The electrochemical reaction is reversible in aqueous solutions and wet [EMIM][NTf$_2$] long exposed to the open air, while it is quasi-reversible in anhydrous [EMIM][NTf$_2$]. Silver ion deposition proceeds without 3D nucleation overvoltage only in acidic aqueous solutions and anhydrous [EMIM][NTf$_2$]. It is shown in particular that back-and-forth scans in SWV allow direct detection of relatively low nucleation overvoltage occurring in 1 M KNO$_3$ solution. The role of the metal-water interface was discussed, kinetic parameters for 0.1 M AgNTf$_2$ in anhydrous [EMIM][NTf$_2$] were determined by numerical simulation and theoretical conclusions on SV for metal ion deposition from high-resistive media previously published were checked.

Key-words

Silver deposition kinetics; Gold electrode; Nitrate solutions; [EMIM][NTf$_2$] ionic liquid; Staircase voltammetry; Square wave voltammetry

1. Introduction

In preceding articles [1-3] staircase voltammetry (SV) and square wave voltammetry (SWV) with metal ion deposition on native and foreign macroelectrodes were studied. In both methods the IR drop was taken into account [2, 3]. Analysis of cyclical SV was concerned with fast and slow simple charge-transfer reactions and consideration was given to the occurrence of 3D nucleation overvoltage [3]. Analysis of SWV was limited to fast reactions and was validated against experimental data for the Ag(I) deposition on a polycrystalline gold disc electrode from acidic nitrate solutions [2].

In the current article, an extended investigation of silver ion deposition on polycrystalline gold and silver disc electrodes of millimetric radius from 1 M HNO_3, 1 M KNO_3 and from anhydrous or wet [EMIM][NTf$_2$] (1-ethyl-3-methyl-1H-imidazol-3-ium bis[(trifluoromethyl)sulfonyl]azanide) room-temperature ionic liquid (RTIL) is presented. The electrochemical reaction has the particularity of being reversible without 3D nucleation in HNO_3, reversible with 3D nucleation in KNO_3 and wet [EMIM][NTf$_2$] left in the open air and quasi-reversible without 3D nucleation in anhydrous [EMIM][NTf$_2$]. Experiments were primarily carried out by SV. The ability to use back-and-forth scans in SWV to detect low nucleation overvoltage is also shown. The present work, apart from its intrinsic interest as an investigation of the Ag(I)/Ag electrode process, especially in AgNTf$_2$-[EMIM][NTf$_2$] solutions, again proves the appropriateness of our modelling approach and confirms the recently accomplished theoretical analysis of cyclical SV with metal ion deposition [3].

We have structured our presentation as follows:
After a brief recall of some mathematical relations, we review bibliographic data regarding the kinetics of the Ag(I)/Ag couple in $HClO_4$ solution and RTILs, physico-chemical properties of anhydrous [EMIM][NTf$_2$] and silver complexes with [EMIM][NTf$_2$]. We then investigate Ag(I) deposition from HNO_3 and KNO_3 solutions. We then investigate Ag(I) deposition from dehydrated [EMIM][NTf$_2$] operated in a glove box under inert conditions. We finally investigate Ag(I) deposition from

[EMIM][NTf$_2$] containing 0.6% of water in equilibrium with the atmospheric water vapour.

2. Recall of some mathematical relations

Modelling of SV and SWV with metal ion deposition and the numerical simulation technique are described in references [2-4]. To compare Ag(I) voltammograms under different experimental conditions, a normalized expression for the current designated as ψ [1-3] was sometimes used. Since the normalization factor in SV is the potential scan rate and in SWV the pulse duration, ψ has two separate forms. For a one-electron deposition reaction on a foreign substrate, ψ as a function of the dimensionless overvoltage $F\eta/RT$ depends, generally, on the adsorption isotherm of metal ions and on a set of dimensionless parameters [1-3] listed below for each method together with ψ expressions:

SV	SWV
$\psi = \dfrac{I}{FAc_{\mathrm{Ox}}^{*}}\sqrt{\dfrac{RT}{FvD_{\mathrm{Ox}}}}$	$\psi = \dfrac{I}{FAc_{\mathrm{Ox}}^{*}}\sqrt{\dfrac{\pi\Delta t}{D_{\mathrm{Ox}}}}$ (individual curves)
$\Delta\mathcal{E}_{\mathrm{s}} = F\lvert\Delta E_{\mathrm{s}}\rvert/RT$	$\Delta\mathcal{E}_{\mathrm{s}} = F\lvert\Delta E_{\mathrm{s}}\rvert/RT$
	$\Delta\mathcal{E} = F\lvert\Delta E\rvert/RT$
$\chi = \dfrac{c_{\mathrm{Ox}}^{*}}{\Gamma_{1}}\sqrt{\dfrac{D_{\mathrm{Ox}}RT}{Fv}}$	$\chi = \dfrac{c_{\mathrm{Ox}}^{*}}{\Gamma_{1}}\sqrt{D_{\mathrm{Ox}}\Delta t}$
$\rho = F^{5/2}R_{\mathrm{u}}\,A\,c_{\mathrm{Ox}}^{*}\left(D_{\mathrm{Ox}}v\right)^{1/2}/(RT)^{3/2}$	$\rho = F^{2}R_{\mathrm{u}}\,A\,c_{\mathrm{Ox}}^{*}\left(D_{\mathrm{Ox}}\right)^{1/2}/(RT\Delta t^{1/2})$
$\psi_{0} = k^{0}\left(\dfrac{RT}{D_{\mathrm{Ox}}Fv}\right)^{1/2}\left(\dfrac{c_{\mathrm{Ox}}^{*}}{c^{0}}\right)^{\alpha_{\mathrm{a}}-1}$	$\psi_{0} = k^{0}\left(\dfrac{\Delta t}{D_{\mathrm{Ox}}}\right)^{1/2}\left(\dfrac{c_{\mathrm{Ox}}^{*}}{c^{0}}\right)^{\alpha_{\mathrm{a}}-1}$
$F\eta_{\mathrm{inv}}/RT$ (backward curve in cyclical SV)	

3

where, A is the surface of the working electrode, c_{Ox}^* the molar bulk concentration of metal ions, D_{Ox} their diffusion coefficient, $|\Delta E_s|$ the height of the steps in the potential staircase in SV and SWV, $|\Delta E|$ the height of the pulses superimposed at the front of each step of the potential staircase in SWV, Δt the pulse duration in SWV (see SWV waveform in reference [2]), Γ_1 the value of the surface concentration Γ of the deposit for which its activity approaches 1, $v = |\Delta E_s|/\Delta t$ the potential scan rate in SV, R_u the uncompensated residual resistance, k^0 the standard charge-transfer rate constant, α_a the anodic charge-transfer coefficient, $c^0 = 1$ mol L^{-1}, η_{inv} the inversion overvoltage in cyclical SV, the remaining symbols having their usual meanings.

The ad hoc adsorption isotherm introduced in calculations is:

$$a_{Red} = 1 - \exp(-4.6\,\Gamma(t)/\Gamma_1) \tag{1}$$

However, we note that for $\chi > 2$, which was mostly the case under our experimental conditions, results do not substantially depend on the isotherm functional form.

Equations used in this work relate to the values of the overvoltage η and of the number ψ at the summit of the forward curve in SV, denoted as η_p and ψ_p, to the overvoltage η_0 of the zero-crossing of the backward curve in cyclical SV and finally to the variation of the overvoltage with time in the galvanostatic step method.

2.1. Staircase voltammetry

2.1.1. Reversible reaction ($\psi_0 \geq 1$) [3]

$$\frac{F\eta_p}{RT} = -0.854 - 0.525\rho - 0.571\left(1 - e^{-\rho^{1.177}}\right) + \Delta\varepsilon_s^{0.467}\left(0.134 - e^{-\left(0.722 + \frac{0.515}{\Delta\varepsilon_s^{1/2}}\right)\rho}\right) \tag{2}$$

$$- \frac{0.34}{\chi\left(1 + 0.65\rho^{2.7}\right)}$$

$$\psi_p = -\frac{0.611}{\left(1 + 0.588\sqrt{\Delta\varepsilon_s}\right)\left(1 + 0.16/\chi\right)} \tag{3}$$

Eq. (3) neglects IR drop effects ($\rho = 0$).

4

$$F|\eta_0|/RT = 8.8165 - 0.7405\,\Delta\mathcal{E}_s^{0.5} - 8.2578\,(F|\eta_{\text{inv}}|/RT)^{-0.08257} \tag{4}$$

2.1.2. Quasi-reversible and irreversible reactions ($\psi_0 < 1$) [3, 5]

$$\alpha_c F\eta_p/RT = -0.780 - \ln\alpha_c/2 + \ln\psi_0 \tag{5}$$

where α_c is the cathodic charge-transfer coefficient.

2.1.3. Irreversible reaction ($\psi_0 \leq 0.01$) [5]

$$\psi_p = -0.4958\sqrt{\alpha_c} \tag{6}$$

Eqs. (5) and (6) neglect IR drop effects.

2.2. Galvanostatic step method (irrespective of the charge-transfer rate) [3, 6]

$$-\frac{I\zeta^{\alpha_c}}{I_0} + \zeta\,a_{\text{Red}} = 1 - \sqrt{t/\tau} \tag{7}$$

Where

I is the constant applied current

$$\zeta = \exp(F\eta/RT) \tag{8}$$

$$I_0 = FAk^0\left(c_{\text{Ox}}^*/c^0\right)^{\alpha_a} c^0 \tag{9}$$

is the exchange current, and

$$\tau = \frac{\pi}{4} D_{\text{Ox}}\left(\frac{FAc_{\text{Ox}}^*}{I}\right)^2 \tag{10}$$

is the transition time.

3. Bibliographic data

Experiments with the Ag(I)/Ag couple were carried out in 1 M HNO_3, 1 M KNO_3 and [EMIM][NTf$_2$] ionic liquid at 25 °C using gold and silver disc electrodes. In this section, bibliographic data on the Ag(I)/Ag couple in $HClO_4$ and various ionic

5

liquids are reviewed. Data concerning [EMIM][NTf$_2$] and its complexes with AgNTf$_2$ are also reviewed.

3.1. HClO$_4$ medium

At 25 °C, the standard potential E^0 of the Ag$^+_{(aq)}$/Ag electrode is 799.1 mV [7]. From galvanostatic double step-function measurements in 1 M HClO$_4$ at 25 °C, the exchange current density I_0/A, for c^*_{Ox} =0.1 M, was found to be (4.5±0.5) A cm^{-2} and α_a =0.74±0.02 [8]. With these values, k^0 from Eq. (9) is (0.26±0.04) cm s^{-1}. Kinetic parameters in 1 M HNO$_3$ should be close to those in 1 M HClO$_4$ because both anions are weakly coordinating.

3.2. Ionic liquids media

3.2.1. AlCl$_3$ (2/3)-[1-butyl-pyridinium]Cl (1/3) and AlCl$_3$ (2/3)-[EMIM]Cl (1/3)

The first study we have listed in ionic liquid medium deals with the coordination of Ag(I) in AlCl$_3$ (2/3)-1-butyl-pyridinium chloride (1/3) and AlCl$_3$ (2/3)-[EMIM][Cl] (1/3) at 40 and 60 °C [9]. Electromotive force measurements with the galvanic cell without liquid junction: $(-)$Al/AlCl$_3$-RCl/fritted disc/AlCl$_3$-RCl, AgCl(dil)/Ag $(+)$, show that Ag(I) forms very stable mononuclear complexes $[AgCl_p]^{1-p}$, $p \in (2, 4)$.

Electrodeposition of silver on platinum, gold and glassy carbon disc electrodes of 0.2 cm^2 and on a tungsten disc electrode of 0.07 cm^2 was investigated by cyclic voltammetry with scan rates between 10 and 200 mV s^{-1}, by stationary voltammetry with rotation of the electrodes and by chronoamperometry (CA) using 1.1x10^{-2} M Ag(I) in AlCl$_3$ (2/3)-[EMIM]Cl (1/3) at 40 °C [10]. At the platinum electrode, the process behaves irreversibly. At the gold electrode, a pre-wave of low intensity develops in positive overvoltages, attributed to the underpotential deposition of silver ion, which interferes with the main wave appearing in negative overvoltages. Three-

6

dimensional nucleation occurs on tungsten (instantaneous) and on glassy carbon (progressive).

3.2.2. AlCl$_3$ (2/3)-[BMIM]Cl (1/3)

Another study of silver deposition on flame annealed Au (1,1,1) films from AlCl$_3$ (2/3) - 1-butyl-3-methyl-1H-imidazol-3-ium chloride (1/3) (or AlCl$_3$ (2/3) - [BMIM]Cl (1/3)) [11] carried out at room temperature by electrochemical scanning tunnelling microscopy, cyclic voltammetry (c_{Ox}^{*} =5x10^{-3} M, v=100 mV s^{-1}) and by CA, highlights the formation of two silver monolayers in the underpotential range. A diffusion controlled deposition of silver layer by layer occurs in the overpotential range without nucleation overvoltage.

Haloaluminate ionic liquids suffered from their high sensitivity to atmospheric moisture and required handling under strict anhydrous conditions to avoid hydrolysis. This disadvantage is largely eliminated with second generation RTILs where imidazolium or pyrrolidinium cations are associated with weakly complexing inorganic and organic anions such as BF$_4$$^-$ and NTf$_2$$^-$ [12].

3.2.3. [EMIM]BF$_4$ and [BMPyr][NTf$_2$]

The kinetics of the Ag(I)/Ag couple in non-haloaluminate RTILs was firstly performed by cyclic voltammetry using a 7.85x10^{-3} cm^2 platinum foil electrode, a 2.1x10^{-2} M AgBF$_4$ solution in [EMIM]BF$_4$ and scan rates lying between 10 and 50 mV s^{-1} [13]. The equilibrium potential as a function of the concentration of Ag (I) follows the Nernst equation but the reduction of Ag(I) is not reversible. The voltammograms were analysed by combining Eqs. (4) and (5) valid for a unidirectional slow reaction which results in D_{Ox}=6x10^{-7} cm^2 s^{-1}, k^0=1x10^{-5} cm s^{-1} and α_c=0.7. A solvodynamic radius of 0.1 nm for the diffusing entity was evaluated from the Stokes-Einstein equation implying that Ag$^+$ is not complexed. We note that the exchange current density of the redox couple must be high enough so that the equilibrium potential is well defined and follows Nernst equation. This is incompatible with a 'totally' irreversible electrochemical reaction. Second, the values of the kinetic parameters

7

found and the potential scan rates used lead to $\psi_0 > 0.14$ which corresponds to a quasi-reversible reaction [3]. In fact, the electrochemical reaction should be quasi-reversible, the diffusion coefficient lower and therefore the solvodynamic radius larger than that found. However, credit can be given to the value of α_c because its calculation from the linear regression slope of the peak potential E_P as a function of $\log v$ (see Eq. (5) and definition of ψ_0 in section 2) is valid for both quasi-reversible and irreversible systems.

The electrochemical kinetics of the Ag(I)/Ag couple was also studied in 1-butyl-1-methylpyrrolidinium bis[(trifluoromethyl)sulfonyl]azanide ([BMPyr][NTf$_2$]) RTIL by cyclic voltammetry at a 10 μm diameter platinum electrode using three different solutions of 8.47×10^{-2} silver trifluoromethanesulfonate (AgOTf), 1.02×10^{-1} M AgNTf$_2$ and 8×10^{-4} M AgNO$_3$ [14]. The reduction process is slow and involves an initial nucleation-controlled stage. The diffusion coefficients of the solutes were determined by CA and are in the sequence as listed: 1.05×10^{-7}, 5.60×10^{-8} and 5.00×10^{-7} cm^2 s^{-1}. The corresponding values of k^0, found by numerical simulation of the backward curves, are: 2×10^{-4}, 1.5×10^{-4} and 0.19×10^{-4} cm s^{-1}. In order to overcome nucleation, the backward curves were simulated individually with a starting potential lower than the inversion potential in the cyclical experiments. The activity of Red was taken constantly equal to 1 and $\alpha_a = \alpha_c = 0.5$.

More recently, the electrodeposition of silver from [EMIM][BF$_4$], dry or wet [BMPyr][NTf$_2$] and from aqueous KNO$_3$ on a glassy carbon electrode was investigated [15]. It was found by cyclic voltammetry that in all cases silver ion deposition proceeds through nucleation-growth kinetics. In the presence of water, the results suggest a possible formation of surface oxides.

3.3. [EMIM][NTf$_2$] selection

[EMIM][NTf$_2$] and [EMIM]BF$_4$ RTILs are among the best suited to study silver electrodeposition since, except for binary haloaluminate ionic liquids, they have at 25 °C the lowest dynamic viscosity (34 and 32 mPa s) and the higher electrical

conductivity (9.2 and 14 mS cm^{-1}) [16]. [EMIM][NTf$_2$] is very slightly soluble in water (1.7x10^{-2} % by weight or 4.4x10^{-4} M at room temperature) [17] and it is commonly characterized as hydrophobic. [EMIM][BF$_4$] is completely soluble in water (hydrophilic). However, the latter has the disadvantage that BF$_4{}^-$ anion undergoes hydrolysis generating HF, even at room temperature [18, 19]. In the presence of 3300 ppm of water, the F$^-$ content at 60 °C is about 400 ppm for [EMIM][BF$_4$] and only 7 ppm for [EMIM][NTf$_2$] [18]. Given these facts, we used [EMIM][NTf$_2$]-AgNTf$_2$ solutions, anhydrous in a glove box under argon and wet in equilibrium with the atmospheric water vapour.

3.4. Some properties of [EMIM][NTf$_2$]

[EMIM][NTf$_2$] is a clear, colourless RTIL with a molar mass M=391.31 g mol^{-1}. Non-matching values for the glass-transition between -98 and -78 °C, the melting point between -3 and -21 °C and the decomposition between 417 and 455 °C, were reported [20]. These differences should mainly be attributed to the degree of purity and water content of the product. For consistency, all water contents we quote were converted into mass fraction in ppm.

The kinetics of the water vapour absorption by [EMIM][NTf$_2$] was studied gravimetrically for relative humidity levels of 43 and 81% at 25 °C under atmospheric pressure [21]. After the first five minutes of exposure, the mass fraction of the absorbed water, c_w, is 244 and 616 ppm, respectively. For 43% humidity, saturation corresponds to c_w=4670 ppm and for 81% humidity it corresponds to c_w=11459 ppm.

Infrared spectroscopy, dielectric spectroscopy and molecular dynamics simulation, suggest that the water present in small quantities in [EMIM][NTf$_2$], is mono-dispersed and linked by hydrogen bonds with the NTf$_2{}^-$ anion [22]. From c_w ≈2300 ppm, water dimers begin to form weakening the water-anion interactions. Water at 458 ppm reduces the mobility of anions while at a ten times greater amount it increases the mobility of both anions and cations.

The effect of the dissolved water on the viscosity of [EMIM][NTf$_2$] was experimentally studied at 25 °C under atmospheric pressure for water contents up to 12590 ppm [23]. From these results, we fitted the following formula for the dynamic viscosity, μ, of [EMIM][NTf$_2$] as a function of its water content c_w (in ppm):

$$\mu = \mu_0 /(1 + 4 \times 10^{-5} c_w) \tag{11}$$

where μ_0 denotes the viscosity of the anhydrous liquid. The standard error of the ratio μ/μ_0 is 0.27x10^{-2}. For c_w=12590 ppm, the relative decrease in viscosity is 33.5%. For dry [EMIM][NTf$_2$] at 25 °C, we selected the value μ_0=(34.3±0.1) mPa s [24]. μ_0 as a function of the temperature T in Kelvin is given with good accuracy by the empirical equation [24]:

$$\mu_0 /(\text{mPa s}) = 0.8423 \exp(9.792 \times 10^7 / T^3) \tag{12}$$

Other formulae for the calculation of μ_0 were also published [25].

A polynomial fit has been proposed for the variation of the natural logarithm of the specific conductivity, κ, as a function of 1/T [25]. The density, ϱ, of [EMIM][NTf$_2$], necessary for calculating the kinematic viscosity $v=\mu/\varrho$ and the molar conductivity $\Lambda=\kappa M/\varrho$, can be computed with an accuracy of five significant digits for T lying between 273.15 and 313.15 K from the following linear fit we have done with the experimental data presented in reference [26]:

$$\varrho/(\text{g cm}^{-3}) = 1.820461 - 1.012762 \times 10^{-3} T \tag{13}$$

The product of conductivity and viscosity of pure [EMIM][NTf$_2$] follows the fractional Walden rule:

$$\Lambda \mu_0^a = Cte \tag{14}$$

with α=0.906 [25]. Thus, with the aid of Eq. (12), we obtain:

$$\frac{1}{\Lambda} \frac{\mathrm{d}\Lambda}{\mathrm{d}T} = -\frac{\alpha}{\mu_0} \frac{\mathrm{d}\mu_0}{\mathrm{d}T} = 2.938 \text{ x} 10^8 \frac{\alpha}{T^4} \tag{15}$$

From Eqs. (15) the temperature coefficients of Λ and μ_0 around 25 °C are 3.4% and -3.7% per degree respectively (Λ increases and μ_0 decreases as the temperature increases). It was found that in RTILs and especially in [EMIM][NTf$_2$] diffusion

10

coefficients can be correlated to the viscosity by the Stokes-Einstein equation writing as [12, 27-29]:

$$D_{Ox} = RT/(4\pi N\mu r) \tag{16}$$

where N is the Avogadro number and r is the solvodynamic radius of the diffusing species. From Eqs. (15) and (16), the temperature coefficient of D_{Ox} is 4% per degree.

Dioxygen has an appreciable solubility in [EMIM][NTf$_2$]. The Henry's law constant was found to be 3.9×10^{-3} M atm^{-1} around 20 °C [30].

3.5. Ag(I) complexes with [EMIM][NTf$_2$]

Ag(I) complexes both with EMIM$^+$ cation [31] and NTf$_2^-$ anion [32] were synthesized and characterized.

Imidazolium cations are precursors of N-heterocyclic carbenes (NHC). When the halide-free [EMIM][NTf$_2$] was treated with an excess of Ag$_2$O at room temperature, three days after there is almost quantitative formation of the corresponding bis-NHC Ag(I) complex. Addition of aqueous KOH accelerates the reaction to quantitative conversion within 16 h [31].

[EMIM][NTf$_2$] blended with AgNTf$_2$ in equimolar amounts yields quantitatively the pure substance [EMIM][Ag(NTf$_2$)$_2$] [32] :

$$[EMIM][NTf_2] + AgNTf_2 = [EMIM][Ag(NTf_2)_2] \tag{17}$$

[EMIM][Ag(NTf$_2$)$_2$] is colourless, has a glass transition temperature of -50 °C, a melting point of 21 °C and decomposes at 392 °C [32]. We can observe that the solubility limit of AgNTf$_2$ in [EMIM][NTf$_2$] is 49.8 % in mass because of the [EMIM][Ag(NTf$_2$)$_2$] quantitative formation. Synthesis of the AgNTf$_2$ compound goes back to the 1990s, but the characterization of its crystal structure is recent [32]. AgNTf$_2$ crystallizes in the triclinic system, has a molar mass of 388.01 g mol^{-1} and a density of 3.035 g cm^{-3} [32].

Coordinating NTf$_2^-$ with Ag$^+$ weakens anion-cation interaction in the solution because hydrogen bonds between the NTf$_2^-$ anion and the proton in position 2 of

11

imidazolium cation are eliminated [32]. Loss of hydrogen bonding interaction could be expected to lead to a reduction in melting point and a decrease in viscosity. However, the melting point of [EMIM][Ag(NTf$_2$)$_2$] is much higher than that of [EMIM][NTf$_2$] and, as we have seen, adding 0.1 M AgNTf$_2$ in [EMIM][NTf$_2$] increased the viscosity from 34.3 to 38.3 mPa s. A similar behaviour was observed with [BMIM]Cl ionic liquid when the imidazolium ring is methylated at position 2 [33]. Indeed, substitution for a methyl group at the 2-position of BMIM$^+$ to form 1-butyl-2,3-dimethyl-imidazol-3-ium leads to an increase both in melting point and in viscosity despite the elimination of the main hydrogen-bonding interaction between the Cl$^-$ anion and the imidazolium cation. It has been hypothesized that the effects due to a loss in hydrogen bonding are outweighed by a loss in entropy caused by a suppression of ion-pair conformers and an increase in the rotational energy barrier of the butyl group, which limits free rotation and facilitates alkyl chain association [33].

4. Instrumentation

The measuring cell of conventional design received a three-electrode assembly and could be thermostated. The auxiliary electrode was a silver wire, rather than a platinum wire which promotes NTf$_2^-$ reduction. The reference electrode was also a silver wire 1 mm in diameter directly immersed in the solution. Electrode potentials were therefore referred to the zero current equilibrium potential of the Ag(I)/Ag couple. The exposed surface of the reference electrode, was chosen to be large, about 1.3 cm^2, in order to increase the intensity of the exchange current in [EMIM][NTf$_2$] where the electrochemical reaction is rather slow. The working electrodes were mainly polycrystalline gold and silver discs, 1 or 2 mm radius, embedded in Teflon cylindrical end caps 6 mm radius being part of the 616 RDE EG&G PARC and EDI101 RADIOMETER ANALYTICAL rotating electrode devices. Current or potential measurements were done in the transient regime without rotating electrodes.

For electrochemical experiments in HNO$_3$ and in wet [EMIM][NTf$_2$] in hygroscopic equilibrium with ambient air, an EG&G PARC 263A potentiostat-galvanostat driven

by the M270 software was used. The uncompensated cell resistance was determined by electrochemical impedance spectroscopy (EIS) with a METROM AUTOLAB PGSTAT30 potentiostat and a frequency response analysis module FRA 4.9 including modelling and fit software of impedance data. For the experiments in dried [EMIM][NTf$_2$], performed under argon in a glove box containing O$_2$ and H$_2$O traces lower than 10^{-6} in molar fraction, a BIOLOGIC VMP3 potentiostat driven by the EC-Lab 10.23 software was used. Dynamic viscosity measurements were done with an ANTON PAAR AMVn falling ball viscometer and density measurements with an ANTON PAAR DSA-5000 densimeter. Water content in [EMIM][NTf$_2$] was determined either by weighing or by Karl Fischer titration using a METTLER TOLEDO V20 coulometer.

5. Preliminary remarks - Working electrode selection

Let us consider usual silver, gold, platinum and glassy carbon solid electrodes in non-complexing aqueous media and dry or wet [EMIM][NTf$_2$]. In this context, the metal ion deposition proceeds without nucleation overvoltage only on silver and gold electrodes in acidic solutions and in anhydrous [EMIM][NTf$_2$]. As an example, in Figs. 1a and 1b voltammograms of AgNO$_3$ in cyclical SV performed in 1 M HNO$_3$ solution at gold, platinum and glassy carbon disc electrodes under the same conditions are shown. At the gold electrode the reduction current starts at the equilibrium potential of the redox couple, while, at the platinum and glassy carbon electrodes a nucleation overvoltage of about -35 mV is obvious in the magnified part of the polarisation curves (Fig. 1b). For these three electrodes, the overvoltage of the zero-crossing of backward curves, η_0, is close to its theoretical value -52 mV predicted by Eq. (4) for reversible systems. Experiments were mainly performed with a gold electrode on which silver ion deposition is reversible without or with 3D nucleation in aqueous solutions and quasi-reversible without 3D nucleation in dry [EMIM][NTf$_2$].
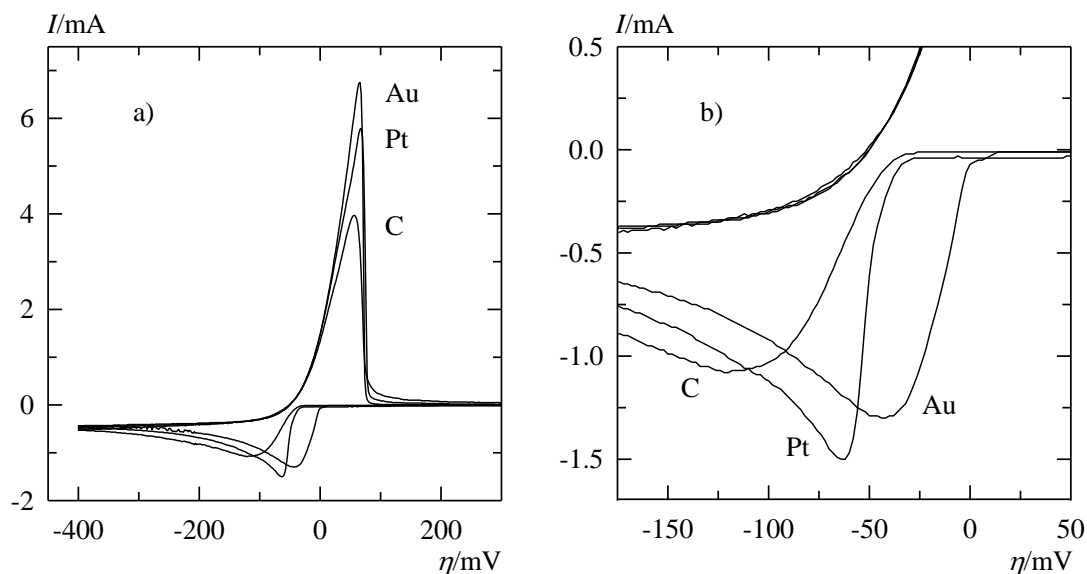
Figs. 1a and 1b. Voltammograms in SV of 3.5×10^{-2} M AgNO$_3$ in 1 M HNO$_3$ at gold, platinum and glassy carbon disc electrodes 2 mm radius. Temperature Θ=25 °C, initial overvoltage η_i =650 mV, inversion overvoltage η_{inv} =-400 mV, step height in the potential staircase $|\Delta E_s|$=2 mV, scan rate v=50 mV s^{-1}. **Fig. 1b** Detailed view of Fig. 1a.

6. Aqueous media

AgNO$_3$ aqueous solutions prepared by weighing in concentrations less than or equal to 3.5×10^{-2} M in 1 M HNO$_3$ and 1 M KNO$_3$ were used. The supporting electrolyte was thus at least in 29-fold excess, sufficient to eliminate contributions from migration [34]. All reagents were analytical grade. AgNO$_3$ powder was dried at 110 °C for 2 hours and then cooled in a desiccator protected from light. Dissolved oxygen was removed by extended bubbling of humidified argon through a bubbler filled with water and the argon stream flow was then kept above the solution. Solutions were thermostated at a temperature Θ=(25±0.1) °C by water circulation. Working disc electrodes were polished by rotary abrasion using RADIOMETER ANALYTICAL abrasive paper 0.3 µm grit size, sonicated and rinsed off thoroughly with ultrapure water.

14

6.1. HNO₃ medium

The validity of theoretical conclusions on SWV was previously proven [2] for the reversible silver ion deposition on the gold disc electrode from acid nitrate media. The new findings presented in this section concern cyclical SV of $AgNO_3$ in 1 M HNO_3 at a polycrystalline gold disc electrode of 2 mm radius.

6.1.1. Physical constants

From the limiting current in stationary SV at a rotating disc electrode, the diffusion coefficient D_{Ox} of $Ag^+_{(aq)}$ in 1 M HNO_3 at 25 °C was found to be $(1.46\pm0.02)\mathrm{x}10^{-5}$ cm^2 s^{-1} [2].

In H_2SO_4 [35] and acid nitrate media [2] two atomic layers of silver are deposited on the gold electrode in the underpotential interval $0<\eta/\mathrm{mV}<600$. The corresponding density of charge passed is 800 μC cm^{-2} [2] and then the surface concentration of silver is $8.29\mathrm{x}10^{-9}$ mol cm^{-2}.

Finally, an uncompensated resistance $R_u = (4\pm0.3)$ Ω in 1 M HNO_3 was fitted from EIS data using the standard Randles equivalent circuit diagram with a constant-phase element for the double layer capacity.

6.1.2. Results in SV and numerical simulation

In SV experiments, two concentrations c_{Ox}^* of $AgNO_3$ $7\mathrm{x}10^{-3}$ and $3.5\mathrm{x}10^{-2}$ M, scan increments $\left|\Delta E_s\right|$ 1 to 8 mV and scan rates v 50 to 200 mV s^{-1} were used. Moreover, to verify the IR modelling, calibrated resistors were connected in series to the working electrode changing R_u from 4 to 336 Ω. Note that this later value is not unusual in RTIL media. Changes in experimental parameters lead to dimensionless parameters settings in the intervals: $0.0389 \leq \Delta\varepsilon_s \leq 0.311$, $1.16 \leq \chi \leq 11.56$ and $0.07 \leq \rho \leq 5.92$.

After polishing and rinsing the electrode, the overall reproducibility of voltammograms has proved satisfactory for ten cycles of silver deposition and dissolution. Before each cyclical potential scan, the electrode was maintained at an

15

initial polarisation overvoltage, η_i , of 650 mV for 40 s to remove residual traces of silver.

The experimental uncertainty on I_p and η_p of the cathodic curve was about $\pm 3\%$ and ± 5 mV, respectively. Given the high intensity of the cathodic peak current, which was between -0.2 and -2.5 mA, the residual current contribution was less than 2%. The reproducibility of the rising part of the anodic curve was excellent. The inclination of the rising part decreases with increasing IR drop. Anodic curve is very sharp and I_p was often poorly defined.

Voltammograms of $AgNO_3$ in SV are plotted in Figs. 2 to 5. The concentration of $AgNO_3$ was 7×10^{-3} M except for Fig. 4 where it was 3.5×10^{-2} M. For voltammograms shown in Fig. 2 only the uncompensated resistance varies. The effect of the IR drop is very pronounced in both position and height of the anodic curves. The numerical simulation of each voltammogram is shown separately in Figs. 3a to 3d. The coincidence of experimental and calculated curves shows that the mastery of IR drop is excellent and therefore the use of macroelectrodes in strongly resistive media presents no disadvantages for the interpretation of our results.
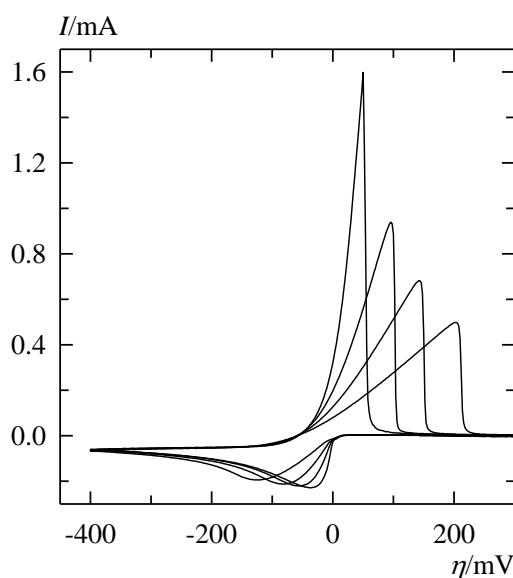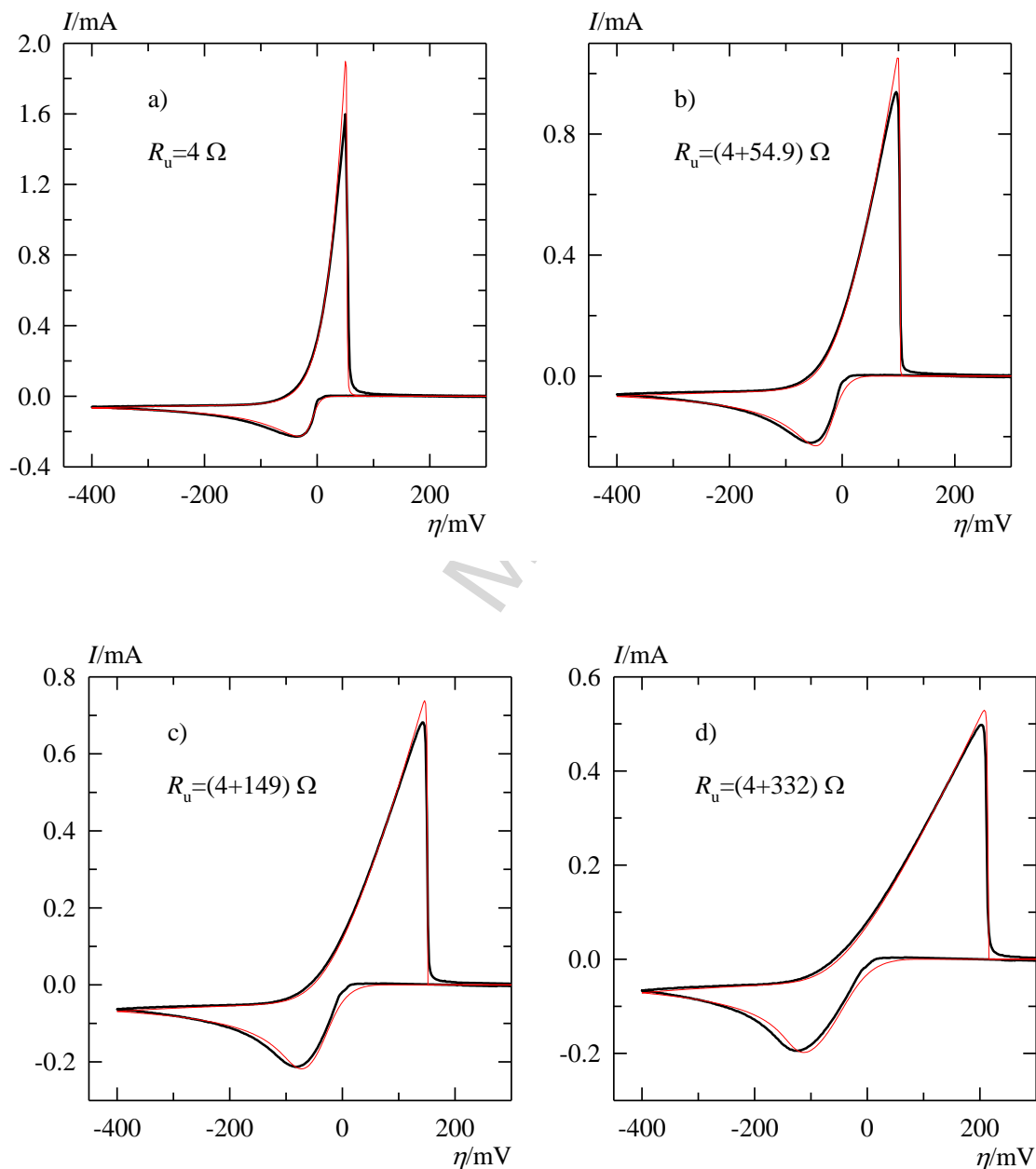

Fig. 2. Effect of variation of the uncompensated resistance R_u in cyclical SV of 7×10^{-3} M $AgNO_3$ in 1 M HNO_3 at the gold disc electrode 2 mm radius. R_u in order of decreasing anodic peak current is: 4, (4+54.9), (4+149) and (4+332) Ω. The second

16

value in parentheses is the ohmic resistance added to the intrinsic value of R_u=4 Ω. Θ=25 °C, η_i =650 mV, η_{inv} =-400 mV, $|\Delta E_s|$=2 mV, v=50 mV s^{-1}.

Figs. 3a to 3d. Simulation of voltammograms in SV plotted in Fig. 2. Experimental voltammograms are plotted in black line and simulated in red line. Θ=25 °C, c_{Ox}^* =7x10^{-3} M, η_i =650 mV, η_{inv} =-400 mV, $|\Delta E_s|$=2 mV ($\Delta\mathcal{E}_s$=0.0778), v=50 mV s^{-1} D_{Ox}=1.46x10^{-5} cm^2 s^{-1}, Γ_1=8.29x10^{-9} mol cm^{-2}, χ=2.31. a) ρ=0.07, b) ρ=1.04, c) ρ=2.69, d) ρ=5.92. The numbers χ and ρ in SV are defined in section 2. The value of R_u is written in each figure.

17

The experimental voltammogram and its simulation shown in Fig. 4 correspond to a high concentration 3.5×10^{-2} M in $AgNO_3$ and a scan rate 200 mV s^{-1}. From calculations we have at $\eta = 12$ mV, i.e. at 31% of the height of the rising part of the anodic curve, $c_{Ox}(x=0)=c_{Ox}^{*}$ and at the anodic vertex overvoltage $c_{Ox}(x=0)=3.3\,c_{Ox}^{*}$. This high concentration at the electrode/solution interface can change the mode of transport by involving migration of Ag^{+}. However, the simulation carried out with the assumption of a purely diffusion-controlled current reproduces well the entire backward curve.
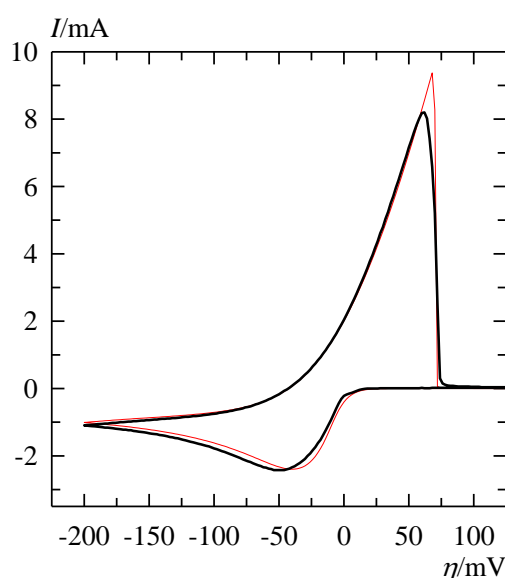

Fig. 4. Experimental (in black line) and simulated (in red line) voltammograms in SV of 3.5×10^{-2} M $AgNO_3$ in 1 M HNO_3 at the gold disc electrode 2 mm radius. $\Theta = 25$ °C, $\eta_i = 650$ mV, $\eta_{inv} = -200$ mV, $|\Delta E_s| = 2$ mV ($\Delta \mathcal{E}_s = 0.0778$), $v = 200$ mV s^{-1}, $D_{Ox} = 1.46 \times 10^{-5}$ cm^2 s^{-1}, $\Gamma_1 = 8.29 \times 10^{-9}$ mol cm^{-2}, $R_u = 4$ Ω, $\chi = 5.78$, $\rho = 0.704$.

To compare the overvoltage of the zero-crossing η_0 in cyclical SV with that predicted from Eq. (4), a series of voltammograms was performed with inversion overvoltages η_{inv} ranging from -100 to -500 mV. Indeed, η_{inv} is the pertinent variable in Eq. (4). For each η_{inv} a same $|\Delta E_s|$ of 2 mV and three scan rates of 50, 100 and 200 mV s^{-1} were used. The sets of voltammograms for the extreme values of η_{inv} are shown in Figs. 5a and 5b. As predicted by the theoretical analysis [3], η_0 is in practice the overvoltage of the crossing point of the backward branches of the cyclical

18

voltammograms recorded with different scan rates. As shown in Table 1, the deviation between experimental and theoretical values of η_0 is lower than 2 mV.
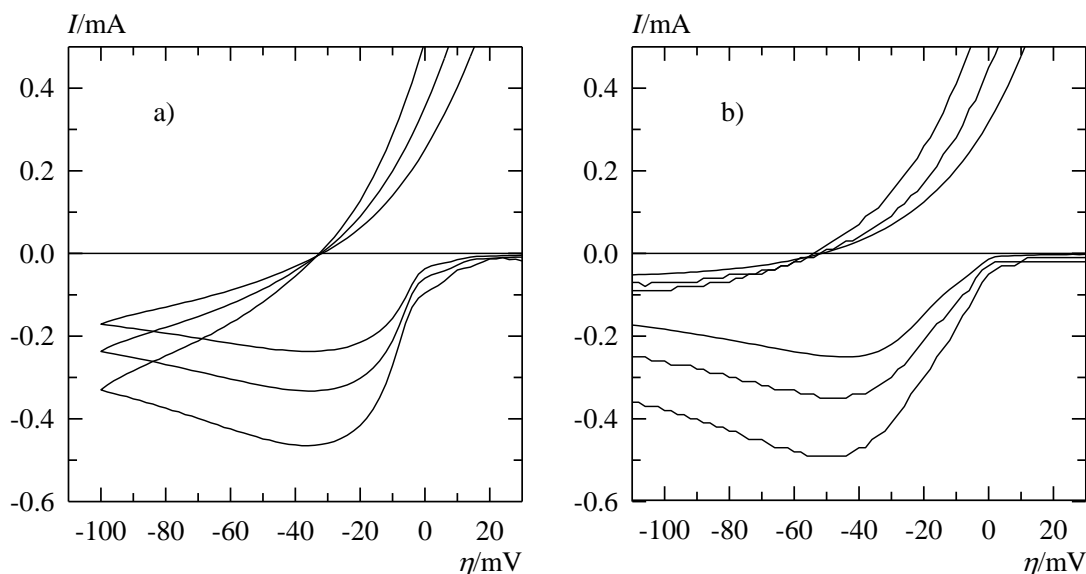
Figs. 5a and 5b. Effect of the inversion overvoltage η_{inv} on the overvoltage of the zero-crossing η_0 in cyclical SV of 7×10^{-3} M AgNO$_3$ in 1 M HNO$_3$ at the disc gold electrode 2 mm radius. Scan rate 50, 100 and 200 mV s^{-1} in order of increasing peak height. Θ=25 °C, η_i =650 mV, $|\Delta E_s|$=2 mV. a) η_{inv} =-100 mV, b) η_{inv} =-500 mV.

Table 1. Experimental values and theoretical values from Eq. (4) of the zero-crossing overvoltage in cyclical SV η_0 for different inversion overvoltages η_{inv} .

$-\eta_{inv}$	η_0/mV Eq. (4)	η_0/mV Experimental
100	31.5	33
200	42.0	42
300	47.9	48
400	51.9	52
500	55.0	56

Finally a set of values of the cathodic η_p and ψ_p, found from several experiments, numerical calculation and the approximate Eqs. (2) and (3), is shown in Table 2.

19

Table 2. η_p /mV and ψ_p found from experiments, numerical simulation and from Eqs. (2) and (3) for different sets of parameters $\Delta\mathcal{E}_s$, χ and ρ.

$\Delta\mathcal{E}_s$	X	ρ	$-\eta_p$ /mV Sim.	$-\eta_p$ /mV Eq. (2)	$-\eta_p$ /mV Exp.	$-\psi_p$ Sim.	$-\psi_p$ Eq. (3)	$-\psi_p$ Exp.
0.0389	2.31	0.07	31.4	31.0	34	0.520	0.512	0.528
0.0778	2.31	0.07	33.0	32.8	36	0.501	0.491	0.506
0.156	2.31	0.07	35.2	35.2	36	0.475	0.464	0.486
0.311	2.31	0.07	38.3	38.6	44	0.442	0.430	0.449
0.0778	1.16	0.14	36.7	37.2	37	0.479	0.461	0.502
0.0778	1.64	0.10	34.7	34.6	35	0.491	0.478	0.505
0.0778	2.31	0.07	33.0	32.8	36	0.501	0.491	0.506
0.0778	5.78	0.704	39.9	40.0	46	0.530	0.511	0.539
0.0778	8.18	0.498	35.8	36.0	42	0.534	0.515	0.550
0.0778	11.56	0.352	33.0	33.3	38	0.536	0.518	0.566
0.0778	2.31	0.07	33.0	32.8	36	0.501	0.491	0.506
0.0778	2.31	1.04	47.1	47.1	53	0.510	0.491	0.491
0.0778	2.31	2.69	72.5	71.7	80	0.482	0.491	0.471
0.0778	2.31	5.92	112.5	115.4	122	0.438	0.491	0.431

It is recalled that Eq. (3) of ψ_p does not account for the IR drop. Using the dimensionless quantity ψ_p instead of I_p, allows us to compare results obtained with different concentrations and scan rates. For the most part, between simulation and experiment, the relative deviation of ψ_p is less than 3% and the absolute deviation of η_p less than 5 mV. The first block of the table from the top shows the influence of $\Delta\mathcal{E}_s$ on η_p and ψ_p. Variation of $\Delta\mathcal{E}_s$ from 0.0389 to 0.311, i.e., of ΔE_s from -1 to -8 mV, causes a decrease of 15% in the height of curves. The third block shows the influence of ρ. The results presented in the intermediate block depend both on χ and ρ. We note that $\left|\psi_p\right|$ ranges from 0.431 to 0.566 and deviates much from 0.611 often used indiscriminately for the analysis of experimental results. This latter value is only

20

valid for metal ion deposition on a native plane electrode in linear voltammetry with true analogue sweep.

6.2. KNO$_3$ medium

Some other experiments were performed with the gold electrode in a 7x10^{-3} M Ag(I)-1 M KNO$_3$ solution. After O$_2$ degassing, the pH of the solution is stabilized at 6.3. At this pH, the hydrolysis of Ag$^+$ is very low [36]. Indeed, the study of the $Ag^+ + H_2O = AgOH + H^+$ equilibrium in 1 M AgNO$_3$ at 25 °C using proton concentration measurements with a glass electrode, showed that pK$_a$ $\geq$11.1 [36]. Therefore, in our Ag(I)-1 M KNO$_3$ solution of same ionic strength, we should have $[AgOH] \leq 10^{-7}$ M. Furthermore, with this solution the uncompensated cell resistance was found to be 14.3 Ω.

In Fig. 6, voltammograms of Ag(I) at the gold electrode in 1 M KNO$_3$ (solid line) and in 1 M HNO$_3$ (dashed line) can be compared. In KNO$_3$, unlike HNO$_3$, a nucleation overvoltage of -33 mV is observed. The difference of 15 mV between anodic peak potentials is due to the difference of 10.3 Ω between R_u values.
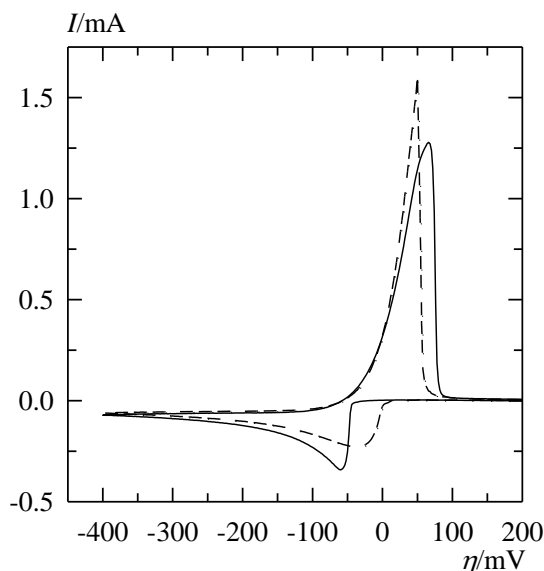

Fig. 6. Voltammograms in SV of 7x10^{-3} M AgNO$_3$ in 1 M KNO$_3$ (solid line) and in 1 M HNO$_3$ (dashed line) at the gold disc electrode 2 mm radius. Θ=25 °C, η_i =650 mV, η_{inv} =-400 mV, $|\Delta E_s|$=2 mV, v=50 mV s^{-1}.

21

To sum up, nucleation overvoltage in the silver ion deposition process on silver and gold electrodes occurs only in neutral aqueous solutions and in hydrated [EMIM][NTf$_2$] RTIL (see section 8 below), i.e., in the presence of adsorbed water dipoles at the electrode surface. Apparently, in acidic solutions co-adsorption of hydronium-water complexes [37] promotes atomic layer deposition of silver and cancels 3D nucleation.

Let $\overline{Q}_{\text{Red}}$ and $\overline{Q}_{\text{Ox}}$ be the apparent charges, in absolute value, calculated for the reduction and oxidation processes in cyclical SV by Simpson's rule integration. We also denote by Q the charge actually transferred during reduction or oxidation in the absence of inhibition of the anodic dissolution. As indicated in our theoretical analysis of SV [3], we have $Q > \overline{Q}_{\text{Red}} > \overline{Q}_{\text{Ox}}$. These three charges tend to equalize as $\Delta \varepsilon_s$ decreases or ρ increases. However, under usual experimental conditions $\overline{Q}_{\text{Ox}}/\overline{Q}_{\text{Red}}$ can be significantly lower than 1. This ratio can only be quantified by integration of simulated curves (without nucleation). Experimental and theoretical values of $\overline{Q}_{\text{Ox}}/\overline{Q}_{\text{Red}}$ in Table 3, show the absence of dissolution inhibition in both HNO$_3$ and KNO$_3$ solutions. In HNO$_3$, where experimental and simulated curves practically coincide (see Fig. 3a), the proximity of the experimental to the theoretical value was expected.

Table 3. Experimental and theoretical ratios $\overline{Q}_{\text{Ox}}/\overline{Q}_{\text{Red}}$ of apparent oxidation and reduction charges for the AgNO$_3$ voltammograms in HNO$_3$ and KNO$_3$ shown in Fig. 6.

Medium	$\overline{Q}_{\text{Ox}}/\overline{Q}_{\text{Red}}$ Experimental	$\overline{Q}_{\text{Ox}}/\overline{Q}_{\text{Red}}$ Theoretical
1 M HNO$_3$	0.90	0.89
1 M KNO$_3$	0.98	0.96

6.2.1. Detection of nucleation overvoltage by SWV

The three-dimensional nucleation overvoltage occurring in the deposition of silver ion onto gold electrode in KNO$_3$ medium is in absolute value lower than $|\eta_0|$

and therefore there is no loop on the cyclic voltammograms in SV. Nucleation is however visible because the current is directly plotted against overvoltage. When an internal metal/metal ion reference electrode is lacking, inspection of the individual curves in SWV performed with distinct potential scans in the negative direction (cathodic scan) and in the positive direction (anodic scan) provides a sensitive criterion for the occurrence of nucleation overvoltage. Analysis of SWV with anodic scans for redox systems having both forms soluble in the liquid phase was presented in references [38-41]. Cathodic scans start at a positive overvoltage where $c_{Ox}(x=0)=c_{Ox}^*$ and anodic scans at a negative overvoltage where $c_{Ox}(x=0)=0$. The differential current has the same sign as ΔE_s and ΔE. For a one-electron reversible metal ion deposition reaction without nucleation, individual curves in SWV implemented with anodic or cathodic scans and $|\Delta E| \geq 40$ mV, are essentially of opposite sign. This is illustrated in Figs. 7a and 7b in which experimental and simulated curves in SWV of AgNO$_3$ in 1 M HNO$_3$ at the gold electrode performed with cathodic (Fig.7a) and anodic (Fig. 7b) scans are presented. The proximity between simulation and experiment is outstanding again.
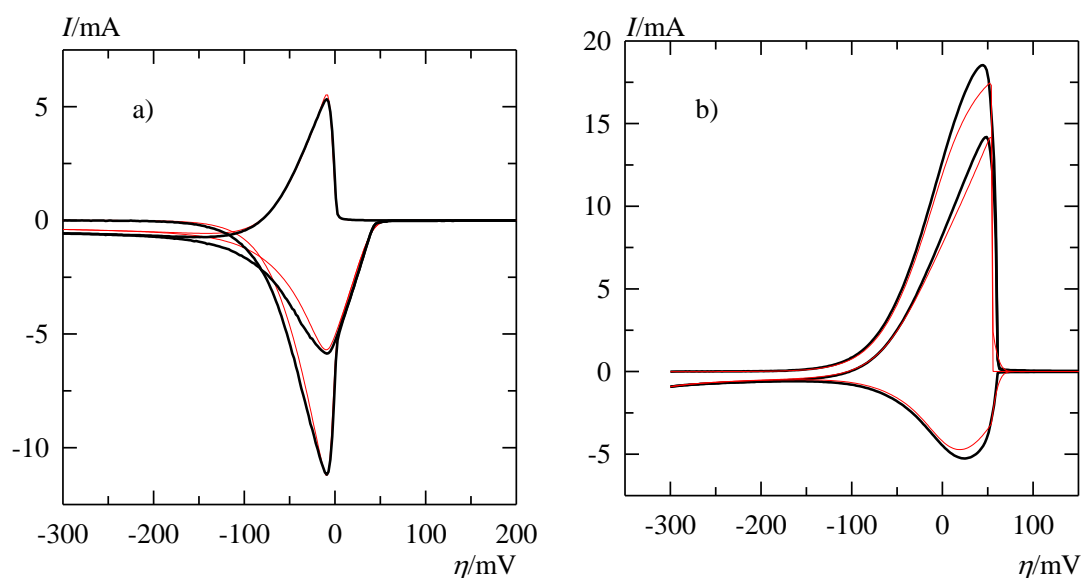
Figs. 7a and 7b. Experimental (in black line) and simulated (in red line) curves in SWV of 3.5x10^{-2} M AgNO$_3$ in 1 M HNO$_3$ at the gold disc electrode 2 mm radius. Θ=25 °C, D_{Ox} =1.46x10^{-5} cm^2 s^{-1}, Γ_1=8.29x10^{-9} mol cm^{-2}, Δt =20 ms, R_u =4 Ω, χ=2.28, ρ=1.79. a) η_i =650 mV, ΔE_s =-2 mV ($\Delta \mathcal{E}_s$=0.0778), ΔE =-80 mV ($\Delta \mathcal{E}$=

3.114). b) η_i =-300 mV, waiting time at η_i =1 s, ΔE_s =2 mV ($\Delta\mathcal{E}_s$ =0.0778), ΔE =80 mV ($\Delta\mathcal{E}$ =3.114). The numbers χ and ρ in SWV are defined in section 2.

In Figs. 8a and 8b curves of $AgNO_3$ in SWV in 1 M KNO_3 at the gold electrode performed respectively with cathodic and anodic scans are presented. Fig. 8a shows that for the cathodic scan, the individual curves in SWV are affected by the nucleation overvoltage which occurs in neutral KNO_3 medium. Indeed, they develop in the negative side of the plane (absence of positive oxidation current at the end of backward pulses in the potential staircase). On the other hand, the peak of the differential curve, which normally should be close to the equilibrium potential, appears at an overvoltage of -45 mV. By cons, for the anodic scan, experimental black curves in Fig. 8b practically coincide with the red curves calculated with the assumption of a reversible reaction without any complication. For emphasis, SWV with a scan towards the positive direction is unaffected by the metal nucleation and provides individual curves of opposite sign.
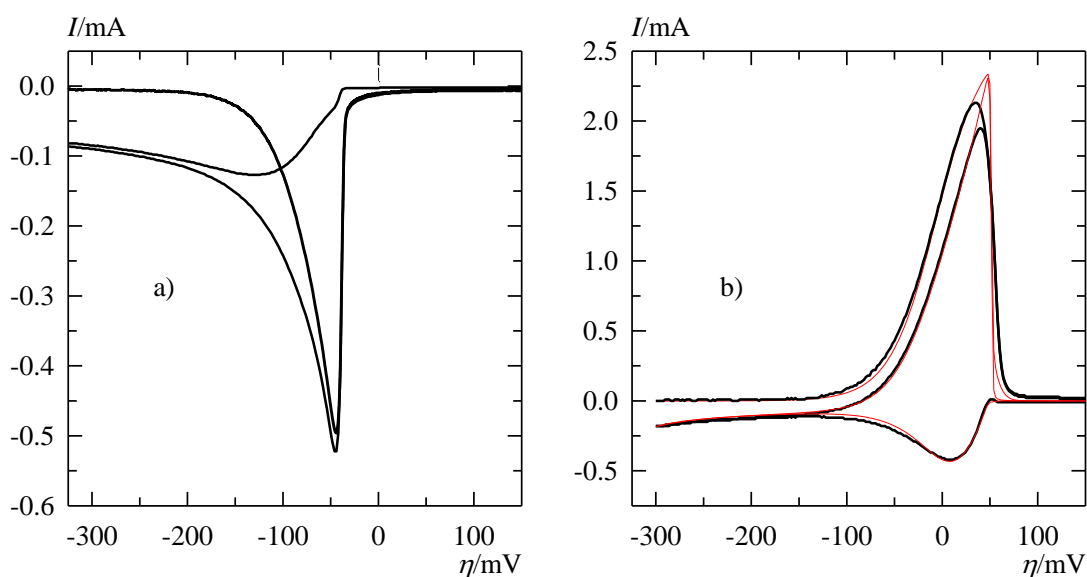
Figs. 8a and 8b. Curves in SWV of 7×10^{-3} M $AgNO_3$ in 1 M KNO_3 at the gold disc electrode 2 mm radius. Experimental curves are plotted in black line and simulated curves in Fig. 8b in red line. Θ=25 °C, Δt =20 ms. a) η_i =650 mV, ΔE_s =-2 mV, ΔE =-40 mV. b) η_i =-300 mV, waiting time at η_i =1 s, ΔE_s =2 mV ($\Delta\mathcal{E}_s$ =0.0778), ΔE =40 mV ($\Delta\mathcal{E}$ =1.557). Additional conditions for the simulation: Reversible reaction, D_{Ox} =1.46$\times10^{-5}$ cm^2 s^{-1}, R_u =14.3 Ω, ρ=1.28, Γ_1 =8.29$\times10^{-9}$ mol cm^{-2}, χ=0.46.

7. Anhydrous [EMIM][NTf$_2$] medium

7.1. General considerations

Solutions were prepared with AgNTf$_2$ 99.5% and halide-free [EMIM][NTf$_2$] 99.9% purity from SOLVIONIC Company. [EMIM][NTf$_2$] was lyophilised before use and its water content, determined by Karl Fischer coulometric titration, never exceeded 150 ppm. Our own measurements of [EMIM][NTf$_2$] viscosity and density gave us average values of 34.2 mPa s and 1.5185 g cm^{-3} consistent with those chosen from bibliographic data in section 3.4. The temperature within the glove box containing the measurement cell was (25±1) °C. Experiments were performed with gold and silver disc electrodes 1 mm radius.

The Ag(I)/Ag electrode reaction in [EMIM][NTf$_2$] is slow and proceeds without nucleation overvoltage. On the other hand, because of the high viscosity of the medium the diffusion coefficient Ag(I) is very low. To study the reaction kinetics, it was necessary to use a relatively high 9.9x10^{-2} M AgNTf$_2$ concentration in order to get a good signal to noise ratio and a fast recovery of the gold electrode surface (χ >2). The uncompensated cell resistance was found by EIS equal to 278 Ω. The viscosity and density of the 9.9x10^{-2} M AgNTf$_2$ solution were found equal to 38.3 mPa s and 1.5322 g cm^{-3}. However, the viscosity of the 10^{-2} M solution in AgNTf$_2$, used to delimit the extent of the electrochemical window, was found substantially identical to that of pure [EMIM][NTf$_2$] (34.3 mPa s) .The unexpected change direction of the viscosity of Ag(I)-[EMIM][NTf$_2$] solutions was commented in Section 3.5. Since in RTIL media the Stokes-Einstein relationship holds [12, 42-44], the necessary conclusion is that the diffusion coefficient of Ag (I) depends on its own concentration.

7.2. Electrochemical window

The electrochemical window of dried [EMIM][NTf$_2$] at the gold electrode (solid curve) for cuts at 0.5 mA cm^{-2} current densities is shown in Fig. 9. In the same figure, the corresponding window at the inert glassy carbon electrode is also shown

25

(dashed curve) to test the hypothesis that the anodic limit on gold is due to the oxidation of the electrode itself [45]. The extent of windows is 4.5 V. The current density in SV is plotted as a function of the overvoltage for a 10^{-2} M Ag(I) concentration which is a standard when the Ag(I)/Ag electrode is used as a reference [46]. Cathodic window limit is due to the one-electron reduction of the EMIM$^+$ cation [46, 47]. NTf$_2$$^-$ anion is also susceptible to cathodic degradation beginning at -1.3 V vs. Fc$^+$/Fc [48-50] or at about -1.7 vs. Ag$^+$ (10^{-2} M)/Ag. To guard against possible reactions involving electrolysis products formed at the limits, separate scans in the negative direction and the positive direction were performed from η_i =600 mV. Cathodic limit for both electrodes is -2.74 V. The anodic limits 1.71 V on glassy carbon and 1.78 V on gold are close. This does not support the assumption of anodic oxidation of the gold electrode in [EMIM][NTf$_2$]. Fig. 9 also shows that Ag(I) reduction peaks are located towards the middle of windows and that on glassy carbon there is a very significant nucleation overpotential of 0.53 V.
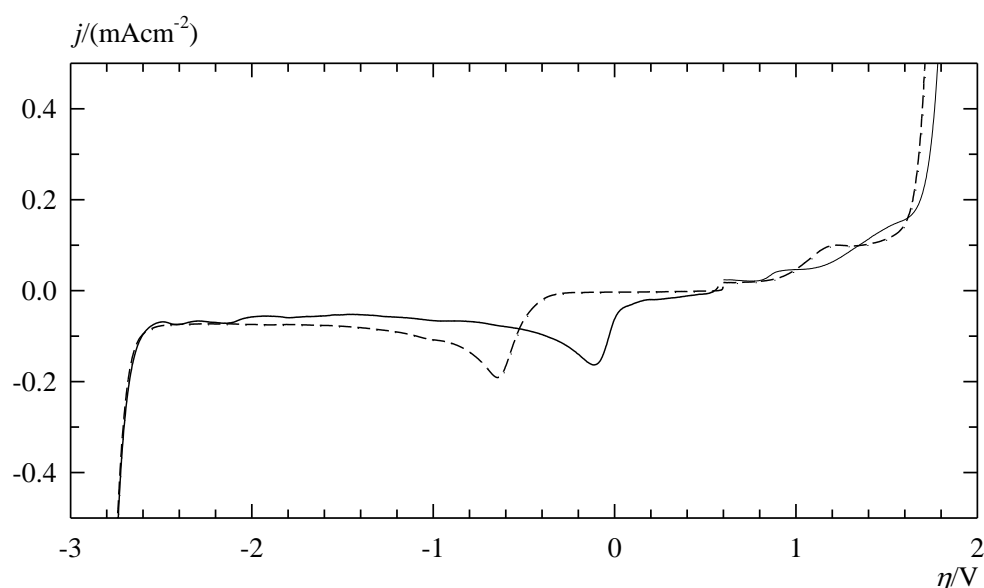

Fig. 9. Electrochemical window at gold (solid line) and glassy carbon (dashed line) disc electrodes 1 mm radius in a 10^{-2} M AgNTf$_2$-[EMIM][NTf$_2$] solution. The current density j in SV is plotted as a function of the overvoltage η for distinct anodic and cathodic scans starting at η_i =600 mV. Θ=25 °C, $|\Delta E_s|$=3 mV and v=50 mVs^{-1}.

26

7.3. Diffusion coefficient of Ag(I)

The diffusion coefficient of Ag(I) at the 9.9×10^{-2} M concentration in [EMIM][NTf$_2$] was determined by CA, stationary voltammetry on rotating electrode being rather ineffective because of the high viscosity of the solution. The current at the gold disc electrode resulting from a potential step at $\eta = -400$ mV follows well the Cottrell equation for a surprisingly long time of one hundred seconds. A change in the initial polarisation overvoltage from 150 to 600 mV does not affect the limiting current. The slope of $I = f(1/\sqrt{t})$ leads to $D_{Ox} = (1.52 \pm 0.05) \times 10^{-7}$ cm^2 s^{-1}.

7.4. On the nature of solute

The molar mass and the density of AgNTf$_2$ are 388.02 g mol^{-1} and 3.035 g cm^{-3} at 25 °C [32]. If AgNTf$_2$ was really the solute, with the usual assumption that its molar volume is the same as in the solid state [51], it should have a solvodynamic radius of 3.7 Å. Using the value of D_{Ox} previously found, the radius of Ag(I) from the Stokes-Einstein equation (15) is 5.7 Å. This result suggests that the value of D_{Ox} should be attributed to $[Ag(NTf_2)_2]^-$ larger than AgNTf$_2$, or to a mixture of these two entities. Finally, the presence of $[Ag(NTf_2)_2]^-$ is supported by the synthesis of [EMIM][Ag(NTf$_2$)$_2$] from AgNTf$_2$ and [EMIM][NTf$_2$] which has a much higher viscosity than that of [EMIM][NTf$_2$] [32].

7.5. Concentration of the underpotential silver deposit

In [EMIM][NTf$_2$] medium, the concentration of silver Γ_1, needed to convert effectively the gold surface to a silver surface of activity $a_{Red} = 1$, was determined by chronopotentiometry. According to Eq. (7), valid whatever k^0, when at time t_1 a_{Red} approaches 1 the variation of the potential versus time becomes substantially linear provided that $t/\tau \ll 1$, τ being the transition time given by Eq. (10). The curve shown in

27

Fig. 10 was obtained by a galvanostatic step-function measurement at the gold disc electrode 1 mm radius in a 0.05 M AgNTf$_2$ solution. After conditioning the electrode for 40 s at η=650 mV, a current of -1 μA was applied. For this current, τ, which in the present case has only a purely theoretical meaning, is 2703 s. Fig.10 shows that the linearity of the response starts at t_1=26 s, which corresponds to 828 μC cm^{-2} charge-density including the charge-density stored in double layer capacity ($\leq$20 μC cm^{-2} [52, 53]). It follows that Γ_1 in [EMIM][NTf$_2$] solution is the same as in HNO$_3$ solution.
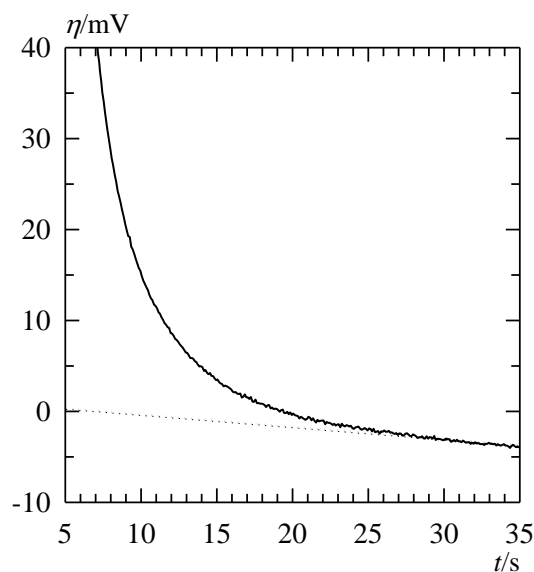

Fig. 10. Variation of the overvoltage η with time t after applying a constant current of -1 μA at the gold disc electrode 1 mm radius in 5x10^{-2} M AgNTf$_2$-[EMIM][NTf$_2$] solution at 25 °C. Conditioning of the electrode at η=650 mV for 40 s. The intersection of the straight dotted line with the experimental solid curve, determines the time t_1 for which the activity a_{Red} reaches 1.

7.6. Experimental results in voltammetry and determination of kinetic parameters

As already indicated, a 9.9x10^{-2} M AgNTf$_2$ solution was used in voltammetry. Fig. 11 shows voltammograms in SV at the gold disc electrode recorded with scan rates of 20, 50 and 100 mV s^{-1} and Fig. 13a, a little further, a voltammogram in SV on the silver disc electrode with a scan rate of 50 mV s^{-1}. In all cases, $|\Delta E_s|$ was 3 mV.
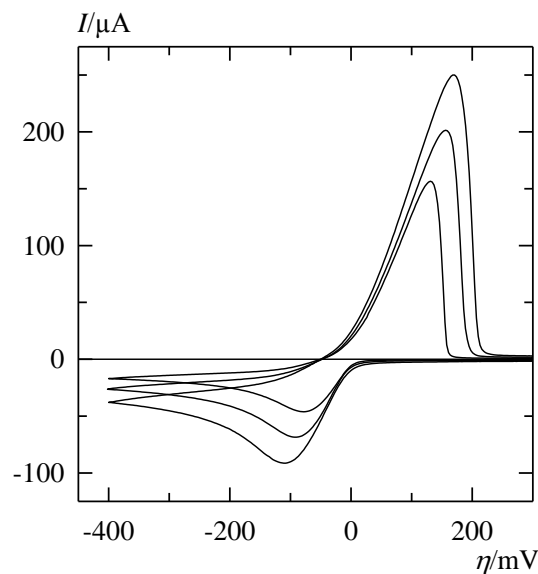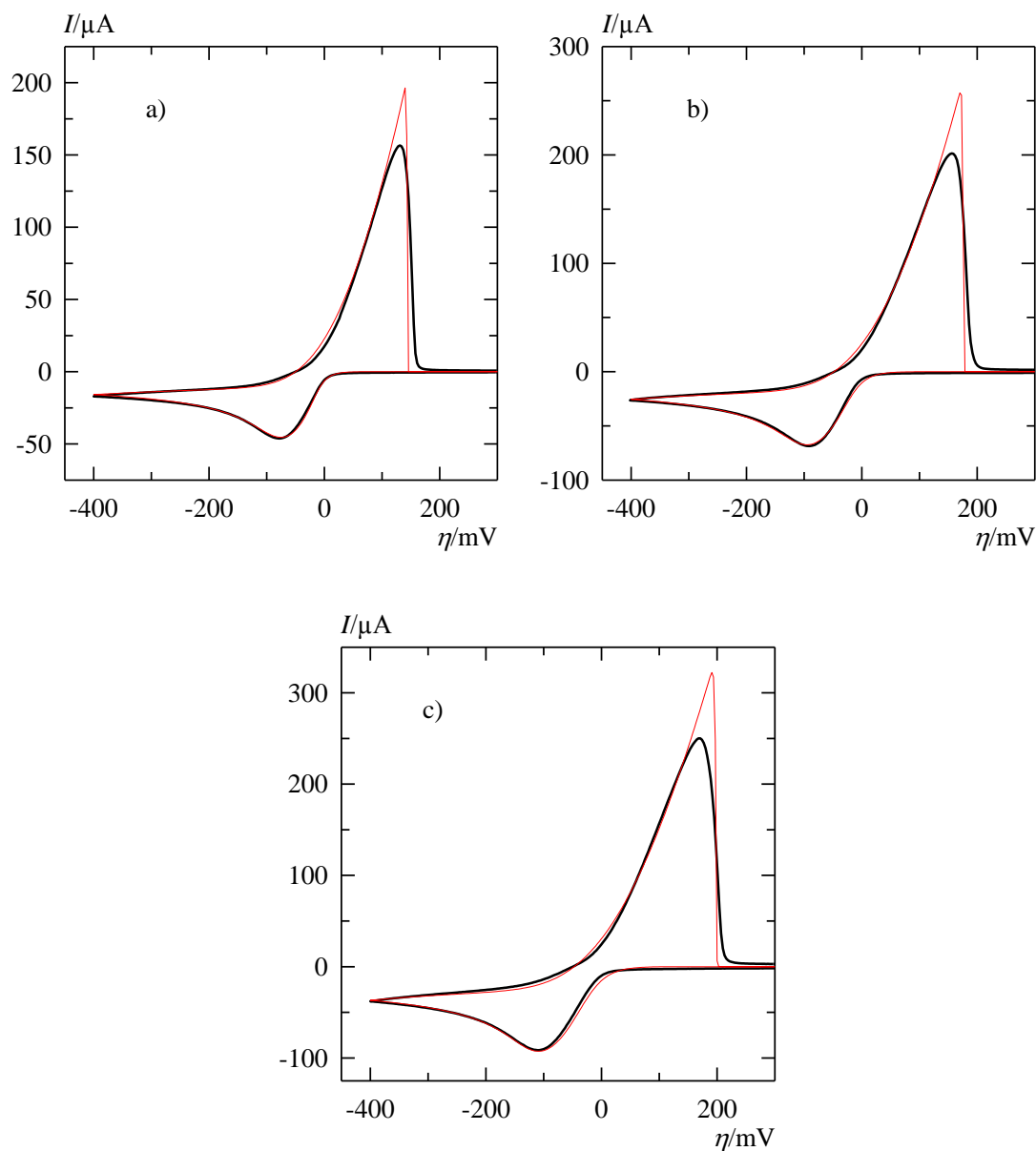
28

Fig. 11. Voltammograms in SV of 9.9×10^{-2} M AgNTf$_2$ in [EMIM][NTf$_2$] at the gold disc electrode 1 mm radius. $\Theta = 25$ °C, $\eta_i = 650$ mV, $\eta_{inv} = -400$ mV, $|\Delta E_s| = 3$ mV. Scan rate: 20, 50 and 100 mV s^{-1} in the order of growth of curves.
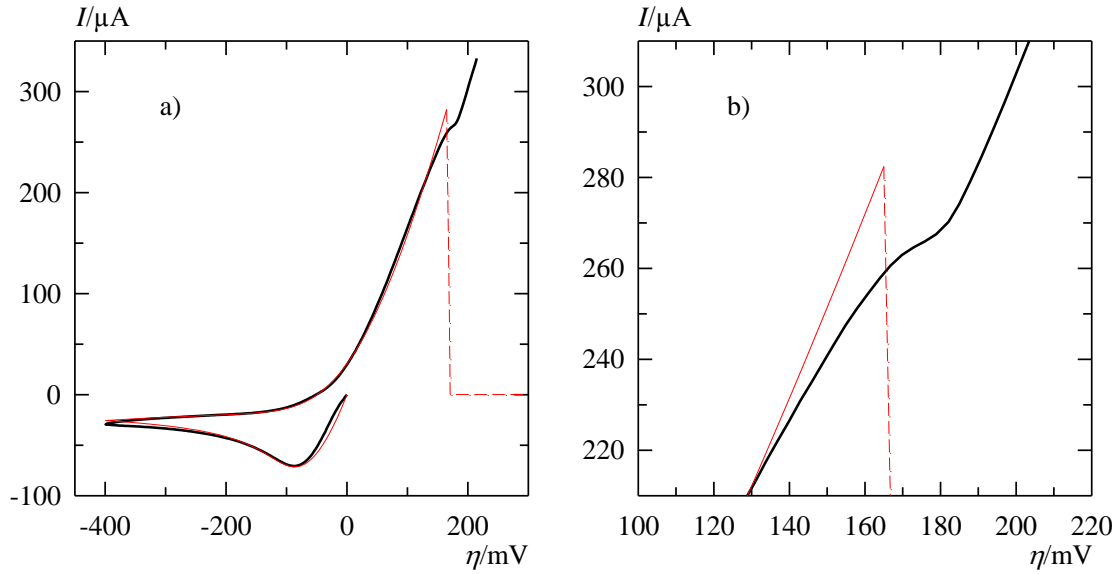
Voltammograms in Fig. 11 were simulated numerically. In fact, the inclination of the rising part of the anodic curve is very sensitive to the value of k^0 and enables its determination by successive iterations taking of course into account the IR drop contribution. On the other side, the morphology and especially the position of the cathodic curve are sensitive to α_c. For the gold electrode, the progressive variation of a_{Red} from 0 to 1 was considered in the model's solution, while for the silver electrode, a_{Red} was taken constantly equal to 1. Assuming that $\alpha_a + \alpha_c = 1$, voltammograms are well reproduced with $\alpha_c = 0.60$, $\alpha_a = 0.40$ and k^0 between 5×10^{-5} and 7×10^{-5} cm s^{-1} as shown in Figs. 12a to 12c, 13a and in Table 4.

With the mean value of k^0, 5.8×10^{-5} cm s^{-1}, we find from Eq. (9) that the exchange current density is 0.89 mA cm^{-2} for $c_{Ox}^* = 10^{-2}$ M and 2.2 mA cm^{-2} for c_{Ox}^* $= 9.9 \times 10^{-2}$ M. The zero-crossing overvoltage η_0 which coincides practically with that of the crossing point of backward curves in Fig. 11 is (48 ± 2) mV. The numerical calculation results in the mean value of $\eta_0 = 48.2$ mV while Eq. (3) for a reversible system gives us 51.9 mV. Fig. 13b shows in particular that after depletion of the superficial silver deposit the oxidation of the structured silver substrate requires an

29

additional overvoltage. Table 4 provides a comparison of experimental and simulated values of η_p and ψ_p of the cathodic curves. The last two columns show the corresponding theoretical values for a reversible system ($\psi_0 \geq 1$).

Figs. 12a to 12c. Simulation of voltammograms shown in Fig. 11. Simulated voltammograms are plotted in red line and experimental voltammograms in black line. $\Theta=25$ °C, $c_{Ox}^{*}=9.9\times10^{-2}$ M, $\eta_i=650$ mV, $\eta_{inv}=-400$ mV, $|\Delta E_s|=3$ mV ($\Delta\mathcal{E}_s=0.117$), $D_{Ox}=1.52\times10^{-7}$ cm^2 s^{-1}, $R_u=278$ Ω, $\Gamma_1=8.29\times10^{-9}$ mol cm^{-2}, $\alpha_c=0.6$ and $\alpha_a=0.4$. a) $v=20$ mV s^{-1}, $k^0=5\times10^{-5}$ cm s^{-1}, $\psi_0=0.582$, $\chi=5.28$, $\rho=1.12$. b) $v=50$ mV s^{-1}, $k^0=5\times10^{-5}$ cm s^{-1}, $\psi_0=0.368$, $\chi=3.34$, $\rho=1.77$. c) $v=100$ mV s^{-1}, $k^0=6\times10^{-5}$ cm s^{-1}, $\psi_0=0.312$, $\chi=2.36$, $\rho=2.50$.
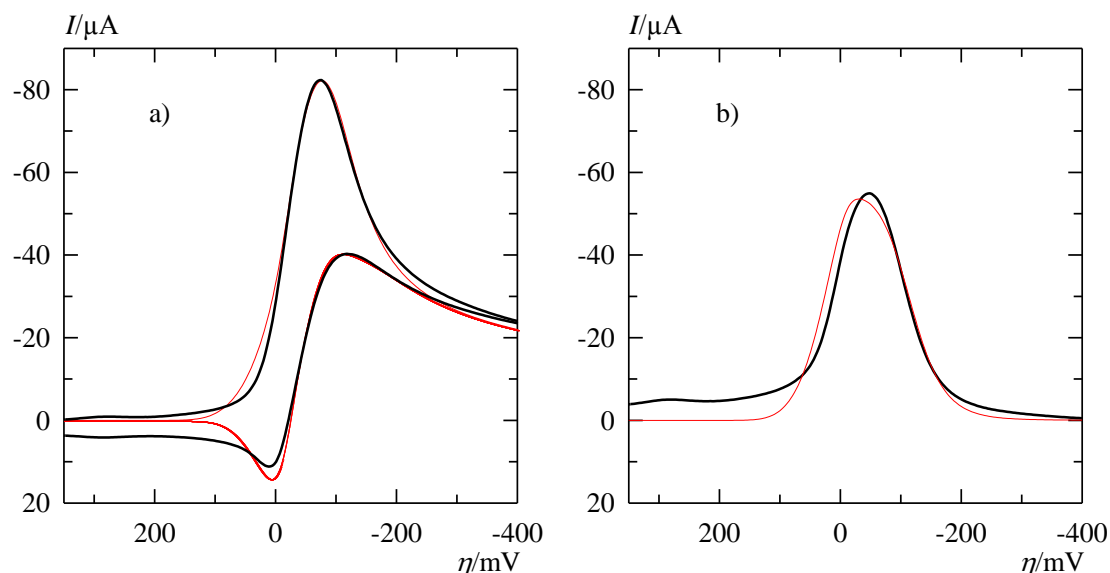
Figs. 13a and 13b. Experimental (in black line) and simulated (in red line) voltammograms in SV of 9.9×10^{-2} M AgNTf$_2$ in [EMIM][NTf$_2$] at the silver disc electrode 1 mm radius. The straight dashed line indicates the abrupt cancellation of the current predicted by the theoretical model which does not take into account the oxidation of the silver substrate after exhaustion of silver adatoms. Θ=25 °C, η_i =0, η_{inv} =-400 mV, $|\Delta E_s|$ =3 mV ($\Delta \mathcal{E}_s$ =0.117), v=50 mV s^{-1}, D_{Ox} =1.52x10^{-7} cm^2 s^{-1}, R_u =278 Ω, k^0 =7x10^{-5} cm s^{-1}, α_c =0.6, α_a =0.4, ψ_0 =0.515, ρ=1.77, a_{Red} =1 $\forall$ t.

Fig. 13b. Detailed view of Fig. 13a showing that the oxidation of the structured silver substrate is more difficult and requires additional overvoltage.

Table 4. η_p /mV and ψ_p of experimental and simulated voltammograms shown in Figs. 12a to 12c and in Fig. 13a for $\Delta \mathcal{E}_s$ =0.117 and different χ, ρ and ψ_0 .The absence of a value for χ corresponds to the bulk silver electrode. The last two columns allow comparison with the reversible case.

χ	ρ	ψ_0	$-\eta_p$ /mV Sim.	$-\eta_p$ /mV Exp.	$-\psi_p$ Sim.	$-\psi_p$ Exp.	$-\eta_p$ /mV Sim. $\psi_0 \geq 1$	$-\psi_p$ Sim. $\psi_0 \geq 1$
2.36	2.50	0.312	108.8	110	0.401	0.396	69.5	0.480
3.34	1.77	0.368	95.0	93	0.416	0.420	58.3	0.497
	1.77	0.515	86.3	87	0.438	0.433	57.6	0.514
5.28	1.12	0.582	75.3	78	0.443	0.448	47.4	0.513

31

Finally, individual and differential curves in SWV at the gold electrode are shown in Figs. 14a and 14b, respectively. The shape of the individual backward curve, that has a positive part, reveals the quasi-reversible character of the electrochemical reaction. Numerical simulation carried out with values of the kinetic parameters found in SV is still in agreement with experiment.

Figs. 14a and 14b. Experimental (in black line) and simulated (in red line) individual (14a) and differential (14b) curves in SWV of 9.9×10^{-2} M $AgNTf_2$ in $[EMIM][NTf_2]$ at the gold disc electrode 1 mm radius. Θ=25 °C, η_i =650 mV, ΔE_s =-3 mV ($\Delta \mathcal{E}_s$ =0.1168), ΔE= -40 mV ($\Delta \mathcal{E}$ =1.557), Δt=40 ms, D_{Ox} =1.52×10^{-7} cm^2 s^{-1}, R_u =278 Ω, Γ_1 =8.29×10^{-9} mol cm^{-2}, k^0 =5×10^{-5} cm s^{-1}, α_c =0.6, α_a =0.4, ψ_0 =0.103, χ=0.93, ρ=6.33. The numbers χ, ρ and ψ_0 in SWV are defined in section 2.

8. Wet $[EMIM][NTf_2]$ medium

8.1. General considerations

Experiments using wet $[EMIM][NTf_2]$, henceforth denoted as $[EMIM][NTf_2]$-H_2O, were performed at (25 ± 0.1) °C with a 5×10^{-2} M $AgNTf_2$ concentration at gold and silver disc electrodes 1 mm radius. The solution was prepared with $[EMIM][NTf_2]$ left in the open air for a week to achieve equilibrium between the ambient water vapour and the water dispersed in the ionic liquid. The day of the experiment, the

water content of [EMIM][NTf$_2$] was 6200 ppm. The viscosity, the density of the solution and the uncompensated cell resistance were found to be 25.3 mPa s, 1.5158 g cm^{-3} and 206 Ω. We note that the proportion of water molecules by silver cation in solution is nearly 10.

8.2. Electrochemical window at the gold electrode

The electrochemical window of [EMIM][NTf$_2$]-H$_2$O at the gold electrode is shown in Fig. 15. The current density in SV with a 10^{-2} M AgNTf$_2$ solution and distinct potential scans in the negative and the positive direction is plotted against overvoltage. The cathodic and anodic limits for cuts at 0.5 mA cm^{-2} are -2.66 V and 1.38 V. The wave of oxygen appears at $\eta \leq$ -1 V and does not interfere with that of Ag(I). It follows that the Ag(I)/Ag couple can be studied safely over a fairly large potential range of 2 V.
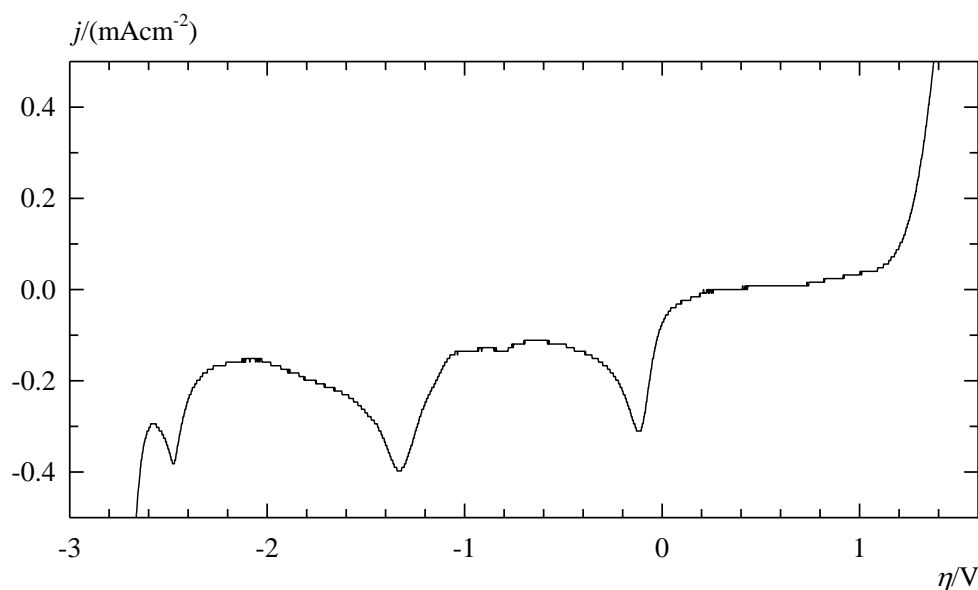

Fig. 15. Electrochemical window at the gold disc electrode 1 mm radius in a 10^{-2} M AgNTf$_2$-[EMIM][NTf$_2$]-H$_2$O solution. The current density j in SV is plotted as a function of the overvoltage η for distinct anodic and cathodic scans starting at η_i =200 mV. Θ=25 °C, $|\Delta E_s|$=2 mV and v=50 mVs^{-1}.

Electrochemical windows in anhydrous and wet [EMIM][NTf$_2$] are in principle not directly comparable because the apparent standard potential of the Ag(I)/Ag couple is not necessarily the same. However, the cathodic limit in [EMIM][NTf$_2$]-H$_2$O

is barely 80 mV higher than that in anhydrous [EMIM][NTf$_2$] (-2.74 V) suggesting that the same species is implicated in both media. As regards the anodic limit, which is significantly lower than that of 1.71 V in anhydrous [EMIM][NTf$_2$], it should be related to the water oxidation.

8.3 Ag(I) diffusion coefficient and solute structure

The diffusion coefficient of Ag(I) in [EMIM][NTf$_2$]-H$_2$O was found by CA at the gold disc electrode. As for anhydrous [EMIM][NTf$_2$], the limiting current-time relationship at η=-300 mV follows the Cottrell equation for several tens of seconds and results in D_{Ox}=3.80x10^{-7} cm^2 s^{-1}. For this value, the Stokes-Einstein radius from Eq. (16) is 3.4 Å significantly lower than that of 5.7 Å in anhydrous [EMIM][NTf$_2$] indicating a change in the structure of the solute. It should be stressed that the average hydrated radius of Ag$^+$ in aqueous solution [54] coincides with that found in [EMIM][NTf$_2$]-H$_2$O. Formation of hydrogen bonds between H$_2$O and NTf$_2$$^-$ anions [22] should significantly weaken or completely disrupt the Ag$^+$ association with these same anions. Moreover, experimental results in SV presented below show that the reaction kinetics of the Ag(I)/Ag couple is greatly accelerated in [EMIM][NTf$_2$]-H$_2$O. On this point, it was justly reported that in aqueous solutions the silver deposition is fast because the hydrated silver cation can approach very close to the electrode surface without losing hydration energy [55]. All of the above discussion reveals that the preponderant Ag(I) solute in [EMIM][NTf$_2$]-H$_2$O should be the hydrated Ag$^+$ cation.

8.4. Experimental results in SV and discussion

Fig. 16 shows voltammograms in SV of 5x10^{-2} AgNTf$_2$ in [EMIM][NTf$_2$]-H$_2$O at the gold disc electrode performed with $|\Delta E_s|$=2 mV and scan rates of 20, 50 and 100 mV s^{-1}. The occurrence of a nucleation overvoltage of -40 mV is clearly visible. The overvoltage η_0 of the crossing point of backward curves is (-49±2) mV. The theoretical value of η_0 for reversible voltammograms with an inversion overvoltage of

34

-300 mV is -48 mV from Eq. (4) and lies within the uncertainty interval of the experimental value, whereas from numerical simulation performed with k^0, α_c and α_a of the quasi-reversible reaction in dried [EMIM][NTf$_2$] a significantly lower value of -43.7 mV is found.
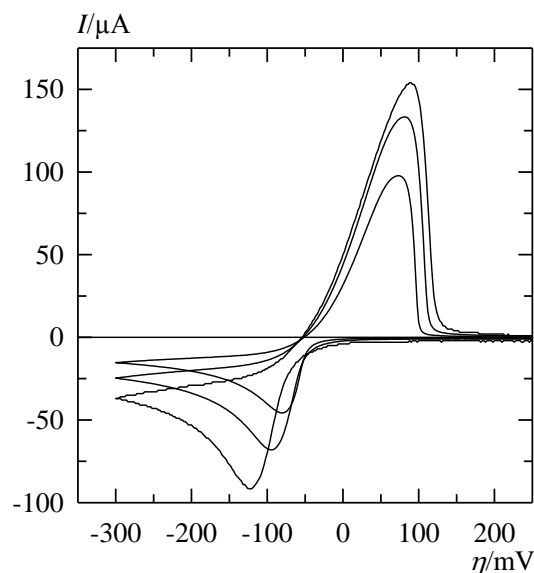

Fig. 16. Voltammograms in SV of 5×10^{-2} M AgNTf$_2$ in [EMIM][NTf$_2$]-H$_2$O at the gold disc electrode 1 mm radius. Θ=25 °C, η_i =650 mV, η_{inv} =-300 mV, $|\Delta E_s|$=2 mV. Scan rate: 20, 50 and 100 mV s^{-1} in the order of growth of curves.

Fig. 17 shows the similarity of the behaviour of voltammograms in SV of 5×10^{-2} M AgNTf$_2$ in [EMIM][NTf$_2$]-H$_2$O at silver and gold electrodes for a scan rate of 50 mV s^{-1}. Under these conditions, the value of χ for the gold electrode, 2.7, is large enough to approximate the behavior of the bulk silver electrode. Integrating anodic and cathodic curves at the gold electrode gives us a ratio of apparent charges $\overline{Q}_{Ox}/\overline{Q}_{Red}$=0.80 while in theory for reversible or quasi-reversible systems without complication this ratio is very close to 1 because of the importance of the IR drop. This finding clearly shows an inhibition of the anodic dissolution of silver probably due to a recovery of the electrode surface by AgOH [15] or by the binuclear species [Ag$_2$OH]$^+$ and Ag$_2$OH$_2$ [36] whose formation should be fast compared to their detachment into solution [56].
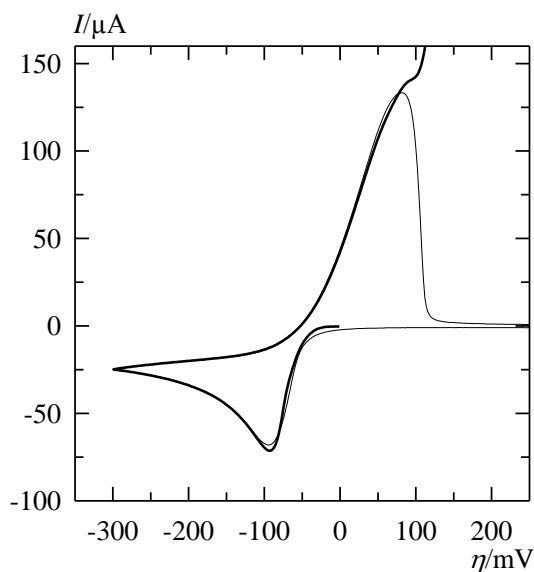
35

Fig. 17. Voltammograms in SV of 5×10^{-2} M AgNTf$_2$ in [EMIM][NTf$_2$]-H$_2$O at silver (in thick line) and gold (in thin line) disc electrodes of 1 mm radius. Θ=25 °C, η_i =650 mV, η_{inv} =-300 mV, $|\Delta E_s|$=2 mV and v=50 mV s^{-1}.

Numerical calculation shows that at equal limiting cathodic current (i.e., $c_{Ox}(0,t)=0$) in SV and CA performed under similar conditions the charge passed is virtually the same. In a first approach, this is easy to ascertain if the concentration profiles are linearized. This property was used to compute independently backward curves in SV.

In Fig. 18, the cyclic voltammogram recorded with v=50 mV s^{-1} and two calculated backward curves, one with the assumption of a reversible charge-transfer (solid red line) and the other with the parameters of the charge-transfer in dried [EMIM][NTf$_2$] (dashed red line), are shown. Calculations were carried out with an initial waiting time of 4.36 s at η=-300 mV in order to obtain the value of the current -24.7 µA observed at this inversion potential in SV. Despite the deformation of the anodic experimental curve due to the inhibition of the silver dissolution, the relative position of calculated curves reveals that the electrochemical reaction in [EMIM][NTf$_2$]-H$_2$O is reversible or very close to the reversibility.
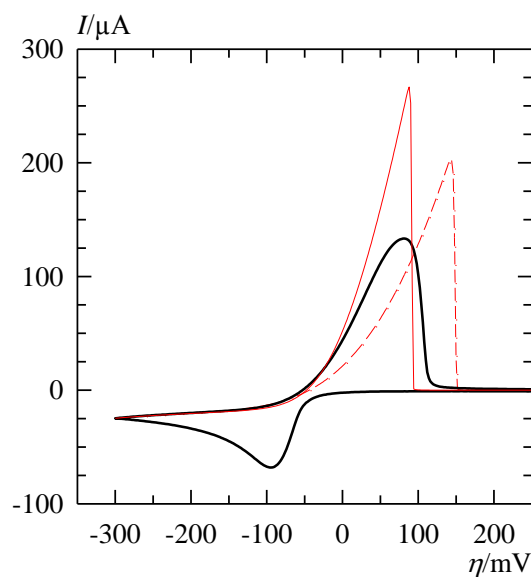
36

Fig. 18. The cyclical voltammogram in black line is that of Fig. 16 achieved with v=50 mV s^{-1}. The backward curve in red solid line was calculated for a reversible reaction and the backward curve in red dashed line for a quasi-reversible reaction with the same values of k^0=5x10^{-5} cm s^{-1}, α_c=0.6 and α_a=0.4 as in anhydrous [EMIM][NTf$_2$]. Other conditions for simulation: Waiting time at -300 mV=4.36 s, Θ=25 °C, $|\Delta E_s|$=2 mV, D_{Ox}=3.80x10^{-7} cm^2 s^{-1}, $\psi_0 \geq 1$ or ψ_0=0.351, R_u=206 Ω, Γ_1=8.29x10^{-9} mol cm^{-2}, χ=2.7 and ρ=1.05.

9. Conclusions

Silver deposition on gold and silver macroelectrodes from aqueous non-complexing solutions and [EMIM][NTf$_2$] RTIL is a good example to be confronted with our theoretical modelling of SV and SWV. Indeed, it may be reversible or quasi-reversible and may proceed with and without 3D nucleation overvoltage. The behaviour of the Ag(I)/Ag couple at gold and silver electrodes is similar except, of course, the consequences due to the gradual recovery of the foreign gold surface especially in low Ag(I) concentration levels.

In RTIL medium of high resistivity taking into account feed-back between current and IR drop in numerical simulation is essential to properly analyse voltammograms in SV and SWV.

37

In the presence of water the overall electrode reaction is identical to the reversible charge-transfer reaction while in anhydrous [EMIM][NTf$_2$] a rate determining bond breaking stage either is detached from the charge-transfer reaction or takes place at the electrode surface. The viscosity of anhydrous solutions of AgNTf$_2$ in [EMIM][NTf$_2$] increases with increasing concentration of AgNTf$_2$ resulting in a decrease of the diffusion coefficient of Ag (I). In a 0.1 M AgNTf$_2$ solution at 25 °C the diffusing entity would be $[Ag(NTf_2)_2]^-$ having a diffusion coefficient of 1.52×10^{-7} cm^2 s^{-1}. For this solution, α_c =0.60, α_a =0.40 and k^0 =5.8×10^{-5} cm s^{-1} were fitted.

Theoretical conclusions on SV and SWV should also be applied very well to liquid metal/metal ion electrodes, e.g. Sn(II)/Sn electrode in LiCl-KCl eutectic melts, where difficulties with heterogeneous nucleation during cathodic metal deposition are no longer encountered.

Finally, the possibility of depositing silver from [EMIM][NTf$_2$] in the open air could initiate an alternative silver-plating process.

References

[1] N. Fatouros, D. Krulic, H. Groult, J. Electroanal. Chem., 625(2009)1-6.

[2] N. Fatouros, D. Krulic, J. Electroanal. Chem., 706(2013)76-85.

[3] D. Krulic, N. Fatouros, D. Liu, J. Electroanal. Chem., 754(2015)30-39.

[4] N. Fatouros, D. Krulic, J. Electroanal. Chem., 443(1998)262-265.

[5] R. S. Nicholson, I. Shain, Anal. Chem. 26(1964)706-723.

[6] K. J. Vetter, Electrochemical Kinetics, theoretical and experimental aspects, Academic Press New-York 1967, p. 207-213.

[7] W. M. Latimer, Oxidation Potentials, Prentice-Hall, lnc. Englewood Cliffs, N. J. 1952, 2. Ed., p. 343.

[8] K. J. Vetter, Electrochemical Kinetics, theoretical and experimental aspects, Academic Press New-York 1967, p. 668.

[9] T. M. Laher, C. L. Hussey, Inorg. Chem. 22(1983)1279-1283.

[10] X.-H. Xu, C. L. Hussey, J. Electrochem. Soc. 139(1992)1295-1300.

[11] C. A. Zell, F. Endres, W. Freyland. Phys. Chem. Chem. Phys., 1 (1999) 697-704.

[12] Ph. Hapiot, C. Lagrost, Chem. Rev. 108(2008)2238–226.

[13] Y. Katayama, S. Dan, T. Miura, T. Kishi, J. Electrochem. Soc. 148(2001)C102-C105.

[14] E. I. Rogers, D. S. Silvester, S. E. Ward Jones, L. Aldous, Ch. Hardacre, A. J. Russell, S. G. Davies, R. G. Compton, J. Phys. Chem. C, 111(2007)13957-13966.

[15] A. Basile, A. I. Bhatt, A. P. O'Mullane, S. K. Bhargava, Electrochimica Acta 56(2011)2895-2905.

[16] Ionic Liquids in Synthesis. Edited by Peter Wasserscheid, Thomas Welton, Wiley-VCH Verlag GmbH & Co. KGaA, Weinheim, 2002, p. 60.

[17] J. M. Crosthwaite, S. N. V. K. Aki, E. J. Maginn, J. F. Brennecke, J. Phys. Chem. B, 108(2004) 5113-5119.

[18] Electrodeposition from Ionic Liquids, Edited by Frank Endres, Douglas MacFarlane et Andrew Abbott, WILEY-VCH Verlag GmbH & Co. KGaA, Weinheim, 2008, p. 25 and 26.

[19] M. G. Freire, C. M. S. S. Neves, I. M. Marrucho, J. A. P. Coutinho,A. M. Fernandes, J. Phys. Chem. A 114(2010)3744–3749.

[20] S. Zhang, N. Sun, X. He, X. Lu, X. Zhang, J. Phys. Chem. Ref. Data, 35(2006)1475-1517.

[21] F. Di Francesco, N. Calisi, M. Creatini, B. Melai, P. Salvo, C. Chiappe, Green Chem. 13(2011)1712-1717.

[22] G. Dimitrakis, I. J. Villar-Garcia, E. Lester, P. Licence, S. Kingman, Phys. Chem. Chem. Phys.10(2008)2947-2951.

[23] J. A. Widegren, A. Laesecke, J. W. Magee, Chem. Commun. (2005)1610-1612.

[24] A. Ahosseini, A. M. Scurto, Int. J. Thermophys. 29(2008)1222-1243.

[25] Ch. Schreiner, S. Zugmann, R. Hartl, H. J. Gores, J. Chem. Eng. Data 55(2010) 4372-4377 and Supporting Information.

[26] A. P. Fröba, H. Kremer, A. Leipertz, J. Phys. Chem. B 112(2008)12420-12430.

[27] L. E. Barrosse-Antle, A. M. Bond, R. G. Compton, A. M. O_Mahony, E. I. Rogers, D. S. Silvester, Chem. Asian J. 5(2010)202–230.

[28] D. S. Silvester, S. Uprety, P. J. Wright, M. Massi, S. Stagni, S. Muzzioli, J. Phys. Chem. C 116(2012)7327−7333.

[29] T. Umecky, Y. Saito, H. Matsumoto, ECS Trans. 25(2010) 23-29.

[30] M. C. Buzzeo, O. V. Klymenko, J. D. Wadhawan, Ch. Hardacre, K. R. Seddon, R. G. Compton, J. Phys. Chem. A 107(2003) 8872-8878.

[31] U. Hintermair, U. Englert, W. Leitner, Organometallics 30(2011)3726-3731.

[32] M. Stricker, B. Oelkers, C. Ph. Rosenau, J. Sundermeyer, Chem. Eur. J. 19(2013)1042-1057 and Supporting Information.

[33] P. A. Hunt, J. Phys. Chem. B, 111(2007)4844-4853.

[34] I. M. Kolthoff and J.J. Lingane, Polarography, volume 1, 2nd edition, Theoretical Principles, Instrumentation and Techniques, Interscience, New-York 1952, p.128.

[35] P. Mrozek, Y. E. Sung, A. Wieckowski, Surface Science, 335(1995)44-51.

[36] G. Biedermann, S. Hietanen, Acta Chem. Scand. 14(1960)711-716.

[37] N. Garcia-Araez, P. Rodriguez, V. Navarro, H. J. Bakker, M. T. M. Koper, J. Phys. Chem. C 115(2011) 21249–21257.

[38] D. Krulic, N. Fatouros, M.M. El Belamachi, J. Electroanal. Chem., 385(1995)33-38.

[39] D. Krulic, N. Fatouros, J. Electroanal. Chem., 520(2002)1-5.

[40] N. Fatouros, D. Krulic, N. Larabi, J. Electroanal. Chem., 549(2003)81-90.

[41] M. Zelic, M. Lovric, J. Electroanal. Chem., 637(2009)28-32.

[42] L. E. Barrosse-Antle, A. M. Bond, R. G. Compton, A. M. O_Mahony, E. I. Rogers, D. S. Silvester, Chem. Asian J. 5(2010)202–230.

[43] D. S. Silvester, S. Uprety, P. J. Wright, M. Massi, S. Stagni, S. Muzzioli, J. Phys. Chem. C 116(2012)7327−7333.

[44] T. Umecky, Y. Saito, H. Matsumoto, ECS Trans. 25(2010) 23-29.

[45] Electrodeposition from Ionic Liquids, Edited by Frank Endres, Douglas MacFarlane and Andrew Abbott, WILEY-VCH Verlag GmbH & Co. KGaA, Weinheim, 2008 p. 156.

[46] Electrochemical Aspects of Ionic Liquids, Edited by Hiroyuki Ohno, John Wiley & Sons, Inc., Hoboken, New Jersey, 2005, p. 40-48.

[47] M. C. Kroon, W. Buijs, C. J. Petersa, G.-J. Witkamp, Green Chem., 8(2006)241-245.

[48] Electrodeposition from Ionic Liquids, Edited by Frank Endres, Douglas MacFarlane and Andrew Abbott, WILEY-VCH Verlag GmbH & Co. KGaA, Weinheim, 2008 p. 158.

[49] F. Endres, S. Zein El Abedin, N. Borissenko, Z. Phys. Chem. 220(2006)1377-1394.

[50] P. C. Howlett, E. I. Izgorodina, M. Forsyth, D. R. MacFarlane, Z. Phys. Chem. 220(2006)1483-1498.

[51] I. M. Kolthoff and J.J. Lingane, Polarography, volume 1, 2nd Edition, Theoretical Principles, Instrumentation and Techniques, Interscience, New-York 1952, p.57.

[52] A. Lewandowski, M. Galinski, S. R. Krajewski, Z. Naturforsch. 62A(2007)187-190.

[53] A. Lewandowski, M. Galinski, S. R. Krajewski, Proceedings of the International Workshop "Portable and Emergency Energy Sources – from Materials to Systems" 16–22 Sept. 2005, Primorsko, Bulgaria.

[54] L. Bruce Railsback, Department of Geology, University of Georgia, Athens, Georgia 30602-2501 U.S.A. "Some Fundamentals of Mineralogy and Geochemistry". http://www.gly.uga.edu/railsback/Fundamentals/8150Speciation08PtIIP.pdf

[55] L. M. C. Pinto, E. Spohr, P. Quaino, E. Santos, W. Schmickler, Angew. Chem. Int. Ed. 52(2013)7883-7885.

[56] W. Stumm, Colloids Surfaces A: Physicochem. Eng. Aspects 120(1997)143-166.

41

Highlights

● Ag(I)/Ag couple at Au and Ag in HNO_3, KNO_3 and dry or wet [EMIM][NTf_2] was studied.

● Conditions to avoid 3D nucleation were specified.

● Kinetic parameters in anhydrous [EMIM][NTf_2] were determined.

● Theory of staircase voltammetry with metal ion deposition was validated.

42